

Azimuthal Asymmetries in DIS as a Probe of Intrinsic Charm Content of the Proton

L.N. Ananikyan* and N.Ya. Ivanov†

Yerevan Physics Institute, Alikhanian Br.2, 375036 Yerevan, Armenia

(Dated: July 4, 2018)

We calculate the azimuthal dependence of the heavy-quark-initiated $\mathcal{O}(\alpha_s)$ contributions to the lepton-nucleon deep inelastic scattering (DIS). It is shown that, contrary to the photon-gluon fusion (GF) component, the photon-quark scattering (QS) mechanism is practically $\cos 2\varphi$ -independent. We investigate the possibility to discriminate experimentally between the GF and QS contributions using their strongly different azimuthal distributions. Our analysis shows that the GF and QS predictions for the azimuthal $\cos 2\varphi$ asymmetry are quantitatively well defined in the fixed flavor number scheme: they are stable, both parametrically and perturbatively. We conclude that measurements of the azimuthal distributions at large Bjorken x could directly probe the intrinsic charm content of the proton. As to the variable flavor number schemes, the charm densities of the recent CTEQ and MRST sets of parton distributions have a dramatic impact on the $\cos 2\varphi$ asymmetry in the whole region of x and, for this reason, can easily be measured.

PACS numbers: 12.38.-t, 13.60.-r, 13.88.+e

Keywords: Perturbative QCD, Heavy Flavor Leptoproduction, Intrinsic Charm, Azimuthal Asymmetries

I. INTRODUCTION

The notion of the intrinsic charm (IC) content of the proton has been introduced over 25 years ago in Refs [1, 2]. It was shown that, in the light-cone Fock space picture [3, 4], it is natural to expect a five-quark state contribution to the proton wave function. The probability to find in a nucleon the five-quark component $|uudcc\rangle$ is of higher twist since it scales as $1/m^2$ where m is the c -quark mass [5]. This component can be generated by $gg \rightarrow c\bar{c}$ fluctuations inside the proton where the gluons are coupled to different valence quarks. Since all of the quarks tend to travel coherently at same rapidity in the $|uudcc\rangle$ bound state, the heaviest constituents carry the largest momentum fraction. For this reason, one would expect that the intrinsic charm component to be dominate the c -quark production cross sections at sufficiently large Bjorken x . So, the original concept of the charm density in the proton [1, 2] has nonperturbative nature and will be referred to in the present paper as nonperturbative IC.

A decade ago another point of view on the charm content of the proton has been proposed in the framework of the variable flavor number scheme (VFNS) [6, 7]. The VFNS is an approach alternative to the traditional fixed flavor number scheme (FFNS) where only light degrees of freedom (u, d, s and g) are considered as active. It is well known that a heavy quark production cross section contains potentially large logarithms of the type $\alpha_s \ln(Q^2/m^2)$ whose contribution dominates at high energies, $Q^2 \rightarrow \infty$. Within the VFNS, these mass logarithms are resummed through the all orders into a heavy quark density which evolves with Q^2 according to the standard DGLAP [8, 9, 10] evolution equation. Hence the VFN schemes introduce the parton distribution functions (PDFs) for the heavy quarks and change the number of active flavors by one unit when a heavy quark threshold is crossed. We can say that the charm density arises within the VFNS perturbatively via the $g \rightarrow c\bar{c}$ evolution and will call it the perturbative IC.

Presently, both perturbative and nonperturbative IC are widely used for a phenomenological description of available data. (A recent review of the theory and experimental constraints on the charm quark distribution can be found in Refs. [11, 12]. See also Appendix C in the present paper). In particular, practically all the recent versions of the CTEQ [13] and MRST [14] sets of PDFs are based on the VFN schemes and contain a charm density. At the same time, the key question remains open: How to measure the intrinsic charm content of the proton? The basic theoretical problem is that radiative corrections to the fixed order predictions for the production cross sections are large. In particular, the next-to-leading order (NLO) corrections increase the leading order (LO) results for both charm and bottom production cross sections by approximately a factor of two at energies of the fixed target experiments. Moreover, soft gluon resummation of the threshold Sudakov logarithms indicates that higher-order contributions are also essential. (For a review see Refs. [15, 16]). On the other hand, perturbative instability leads to a high sensitivity of the theoretical

*Electronic address: lev@web.am

†Electronic address: nikiv@uniphi.yerphi.am

calculations to standard uncertainties in the input QCD parameters. For this reason, it is difficult to compare pQCD results for spin-averaged cross sections with experimental data directly, without additional assumptions. The total uncertainties associated with the unknown values of the heavy quark mass, m , the factorization and renormalization scales, μ_F and μ_R , Λ_{QCD} and the PDFs are so large that one can only estimate the order of magnitude of the pQCD predictions for production cross sections [17, 18].

Since production cross sections are not perturbatively stable, it is of special interest to study those observables that are well-defined in pQCD. A nontrivial example of such an observable was proposed in Refs. [19, 20, 21, 22] where the azimuthal $\cos 2\varphi$ asymmetry in heavy quark photo- and lepton production has been analyzed¹. In particular, the Born level results have been considered [19] and the NLO soft-gluon corrections to the basic mechanism, photon-gluon fusion (GF), have been calculated [20, 21]. It was shown that, contrary to the production cross sections, the azimuthal asymmetry in heavy flavor photo- and lepton production is quantitatively well defined in pQCD: the contribution of the dominant GF mechanism to the asymmetry is stable, both parametrically and perturbatively. Therefore, measurements of this asymmetry would provide an ideal test of pQCD. As was shown in Ref. [22], the azimuthal asymmetry in open charm photoproduction could have been measured with an accuracy of about ten percent in the approved E160/E161 experiments at SLAC [23] using the inclusive spectra of secondary (decay) leptons.

In the present paper we study the IC contribution to the azimuthal asymmetries in heavy quark lepton production:

$$l(\ell) + N(p) \rightarrow l(\ell - q) + Q(p_Q) + X[\bar{Q}](p_X). \quad (1)$$

Neglecting the contribution of Z -boson as well as the target mass effects, the cross section of the reaction (1) for unpolarized initial states may be written as

$$\frac{d^3\sigma_{lN}}{dx dQ^2 d\varphi} = \frac{\alpha_{em}}{(2\pi)^2} \frac{1}{x Q^2} \frac{y^2}{1 - \varepsilon} \left[\sigma_T(x, Q^2) + \varepsilon \sigma_L(x, Q^2) + \varepsilon \sigma_A(x, Q^2) \cos 2\varphi + 2\sqrt{\varepsilon(1 + \varepsilon)} \sigma_I(x, Q^2) \cos \varphi \right], \quad (2)$$

The quantity ε measures the degree of the longitudinal polarization of the virtual photon in the Breit frame [24],

$$\varepsilon = \frac{2(1 - y)}{1 + (1 - y)^2}, \quad (3)$$

and the kinematic variables are defined by

$$\begin{aligned} \bar{S} &= (\ell + p)^2, & Q^2 &= -q^2, & x &= \frac{Q^2}{2p \cdot q}, \\ y &= \frac{p \cdot q}{p \cdot \ell}, & Q^2 &= xy\bar{S}, & \rho &= \frac{4m^2}{\bar{S}}. \end{aligned} \quad (4)$$

The cross sections σ_i ($i = T, L, A, I$) in Eq. (2) are related to the structure functions $F_i(x, Q^2)$ as follows:

$$\begin{aligned} F_i(x, Q^2) &= \frac{Q^2}{8\pi^2 \alpha_{em} x} \sigma_i(x, Q^2), \quad (i = T, L, A, I) \\ F_2(x, Q^2) &= \frac{Q^2}{4\pi^2 \alpha_{em}} \sigma_2(x, Q^2), \end{aligned} \quad (5)$$

where $F_2 = 2x(F_T + F_L)$ and $\sigma_2 = \sigma_T + \sigma_L$. In Eq. (2), σ_T (σ_L) is the usual $\gamma^* N$ cross section describing heavy quark production by a transverse (longitudinal) virtual photon. The third cross section, σ_A , comes about from interference between transverse states and is responsible for the $\cos 2\varphi$ asymmetry which occurs in real photoproduction using linearly polarized photons [19, 20, 22]. The fourth cross section, σ_I , originates from interference between longitudinal and transverse components [24]. In the nucleon rest frame, the azimuth φ is the angle between the lepton scattering plane and the heavy quark production plane, defined by the exchanged photon and the detected quark Q (see Fig. 1). The covariant definition of φ is

$$\cos \varphi = \frac{r \cdot n}{\sqrt{-r^2} \sqrt{-n^2}}, \quad \sin \varphi = \frac{Q^2 \sqrt{1/x^2 + 4m_N^2/Q^2}}{2\sqrt{-r^2} \sqrt{-n^2}} n \cdot \ell, \quad (6)$$

$$r^\mu = \varepsilon^{\mu\nu\alpha\beta} p_\nu q_\alpha \ell_\beta, \quad n^\mu = \varepsilon^{\mu\nu\alpha\beta} q_\nu p_\alpha p_{Q\beta}. \quad (7)$$

¹ The well-known examples are the shapes of differential cross sections of heavy flavor production which are sufficiently stable under radiative corrections.

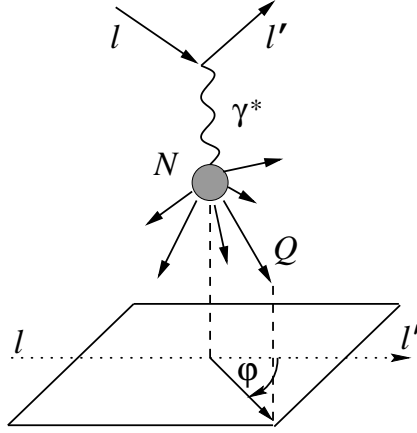


FIG. 1: Definition of the azimuthal angle φ in the nucleon rest frame.

In Eqs. (4) and (6), m and m_N are the masses of the heavy quark and the target, respectively. Usually, the azimuthal asymmetry associated with the $\cos 2\varphi$ distribution, $A_{2\varphi}(\rho, x, Q^2)$, is defined by

$$\begin{aligned} A_{2\varphi}(\rho, x, Q^2) &= 2\langle \cos 2\varphi \rangle(\rho, x, Q^2) = \frac{d^3\sigma_{lN}(\varphi = 0) + d^3\sigma_{lN}(\varphi = \pi) - 2d^3\sigma_{lN}(\varphi = \pi/2)}{d^3\sigma_{lN}(\varphi = 0) + d^3\sigma_{lN}(\varphi = \pi) + 2d^3\sigma_{lN}(\varphi = \pi/2)} \\ &= \frac{\varepsilon \sigma_A(x, Q^2)}{\sigma_T(x, Q^2) + \varepsilon \sigma_L(x, Q^2)} = A(x, Q^2) \frac{\varepsilon + \varepsilon R(x, Q^2)}{1 + \varepsilon R(x, Q^2)}, \end{aligned} \quad (8)$$

where $d^3\sigma_{lN}(\varphi) = \frac{d^3\sigma_{lN}}{dx dQ^2 d\varphi}(\rho, x, Q^2, \varphi)$ and the mean value of $\cos n\varphi$ is

$$\langle \cos n\varphi \rangle(\rho, x, Q^2) = \frac{\int_0^{2\pi} d\varphi \cos n\varphi \frac{d^3\sigma_{lN}}{dx dQ^2 d\varphi}(\rho, x, Q^2, \varphi)}{\int_0^{2\pi} d\varphi \frac{d^3\sigma_{lN}}{dx dQ^2 d\varphi}(\rho, x, Q^2, \varphi)}. \quad (9)$$

In Eq. (8), the quantities $R(x, Q^2)$ and $A(x, Q^2)$ are defined as

$$R(x, Q^2) = \frac{\sigma_L}{\sigma_T}(x, Q^2) = \frac{F_L}{F_T}(x, Q^2), \quad (10)$$

$$A(x, Q^2) = \frac{\sigma_A}{\sigma_2}(x, Q^2) = 2x \frac{F_A}{F_2}(x, Q^2). \quad (11)$$

Likewise, we can define the azimuthal asymmetry associated with the $\cos \varphi$ distribution, $A_\varphi(\rho, x, Q^2)$:

$$\begin{aligned} A_\varphi(\rho, x, Q^2) &= 2\langle \cos \varphi \rangle(\rho, x, Q^2) = \frac{2d^3\sigma_{lN}(\varphi = 0) - 2d^3\sigma_{lN}(\varphi = \pi)}{d^3\sigma_{lN}(\varphi = 0) + d^3\sigma_{lN}(\varphi = \pi) + 2d^3\sigma_{lN}(\varphi = \pi/2)} \\ &= \frac{2\sqrt{\varepsilon(1+\varepsilon)} \sigma_I(x, Q^2)}{\sigma_T(x, Q^2) + \varepsilon \sigma_L(x, Q^2)} = A_I(x, Q^2) \sqrt{\varepsilon(1+\varepsilon)/2} \frac{1 + R(x, Q^2)}{1 + \varepsilon R(x, Q^2)}, \end{aligned} \quad (12)$$

where

$$A_I(x, Q^2) = 2\sqrt{2} \frac{\sigma_I}{\sigma_2}(x, Q^2) = 4\sqrt{2} x \frac{F_I}{F_2}(x, Q^2). \quad (13)$$

Remember that $y \ll 1$ in most of the experimentally reachable kinematic range. Taking also into account that $\varepsilon = 1 + \mathcal{O}(y^2)$, we find:

$$A_{2\varphi}(\rho, x, Q^2) = A(x, Q^2) + \mathcal{O}(y^2), \quad A_\varphi(\rho, x, Q^2) = A_I(x, Q^2) + \mathcal{O}(y^2). \quad (14)$$

So, like the $\sigma_2(x, Q^2)$ cross section in the φ -independent case, it is the parameters $A(x, Q^2)$ and $A_I(x, Q^2)$ that can effectively be measured in the azimuthal-dependent production.

In this paper we concentrate on the azimuthal asymmetry $A(x, Q^2)$ associated with the $\cos 2\varphi$ -distribution. We have calculated the IC contribution to the asymmetry which is described at the parton level by the photon-quark scattering (QS) mechanism given in Fig. 2. Our main result can be formulated as follows:

- Contrary to the basic GF component, the IC mechanism is practically $\cos 2\varphi$ -independent. This is due to the fact that the QS contribution to the $\sigma_A(x, Q^2)$ cross section is absent (for the kinematic reason) at LO and is negligibly small (of the order of 1%) at NLO.

As to the φ -independent cross sections, our parton level calculations have been compared with the previous results for the IC contribution to $\sigma_2(x, Q^2)$ and $\sigma_L(x, Q^2)$ presented in Refs. [25, 26]. Apart from two trivial misprints uncovered in [25] for $\sigma_L(x, Q^2)$, a complete agreement between all the considered results is found.

Since the GF and QS mechanisms have strongly different $\cos 2\varphi$ -distributions, we investigate the possibility to discriminate between their contributions using the azimuthal asymmetry $A(x, Q^2)$. We analyze separately the non-perturbative IC in the framework of the FFNS and the perturbative IC within the VFNS.

The following properties of the nonperturbative IC contribution to the azimuthal asymmetry within the FFNS are found:

- The nonperturbative IC is practically invisible at low x , but affects essentially the GF predictions at large x . The dominance of the $\cos 2\varphi$ -independent IC component at large x leads to a more rapid (in comparison with the GF predictions) decreasing of $A(x, Q^2)$ with growth of x .
- Contrary to the production cross sections, the $\cos 2\varphi$ asymmetry in charm azimuthal distributions is practically insensitive to radiative corrections at $Q^2 \sim m^2$. Perturbative stability of the combined GF+QS result for $A(x, Q^2)$ is mainly due to the cancellation of large NLO corrections in Eq. (11).
- pQCD predictions for the $\cos 2\varphi$ asymmetry are parametrically stable; the GF+QS contribution to $A(x, Q^2)$ is practically insensitive to most of the standard uncertainties in the QCD input parameters: μ_R , μ_F , Λ_{QCD} and PDFs.
- Nonperturbative corrections to the charm azimuthal asymmetry due to the gluon transverse motion in the target are of the order of 20% at $Q^2 \leq m^2$ and rapidly vanish at $Q^2 > m^2$.

We conclude that the contributions of both GF and IC components to the $\cos 2\varphi$ asymmetry in charm leptoproduction are quantitatively well defined in the FFNS: they are stable, both parametrically and perturbatively, and insensitive (at $Q^2 > m^2$) to the gluon transverse motion in the proton. At large Bjorken x , the $A(x, Q^2)$ asymmetry could be a sensitive probe of the nonperturbative IC.

The perturbative IC has been considered within the VFNS proposed in Refs. [6, 7]. The following features of the azimuthal asymmetry should be emphasized:

- * Contrary to the nonperturbative IC component, the perturbative one is significant practically at all values of Bjorken x and $Q^2 > m^2$.
- * The charm densities of the recent CTEQ and MRST sets of PDFs lead to a sizeable reduction (by about 1/3) of the GF predictions for the $\cos 2\varphi$ asymmetry.

We conclude that impact of the perturbative IC on the $\cos 2\varphi$ asymmetry is sizeable in the whole region of x and, for this reason, can easily be detected.

Concerning the experimental aspects, azimuthal asymmetries in charm leptoproduction can, in principle, be measured in the COMPASS experiment at CERN, as well as in future studies at the proposed eRHIC [27, 28] and LHeC [29] colliders at BNL and CERN, correspondingly.

The paper is organized as follows. In Section II we analyze the QS and GF parton level predictions for the φ -dependent charm leptoproduction in the single-particle inclusive kinematics. In particular, we discuss our results for the NLO QS cross sections and compare them with available calculations. Hadron level predictions for $A(x, Q^2)$ are given in Section III. We consider the IC contributions to the asymmetry within the FFNS and VFNS in a wide region of x and Q^2 . Some details of our calculations of the QS cross sections are presented in Appendix A. An overview of the soft-gluon resummation for the photon-gluon fusion mechanism is given in Appendix B. Some experimental facts in favor of the nonperturbative IC are briefly listed in Appendix C.

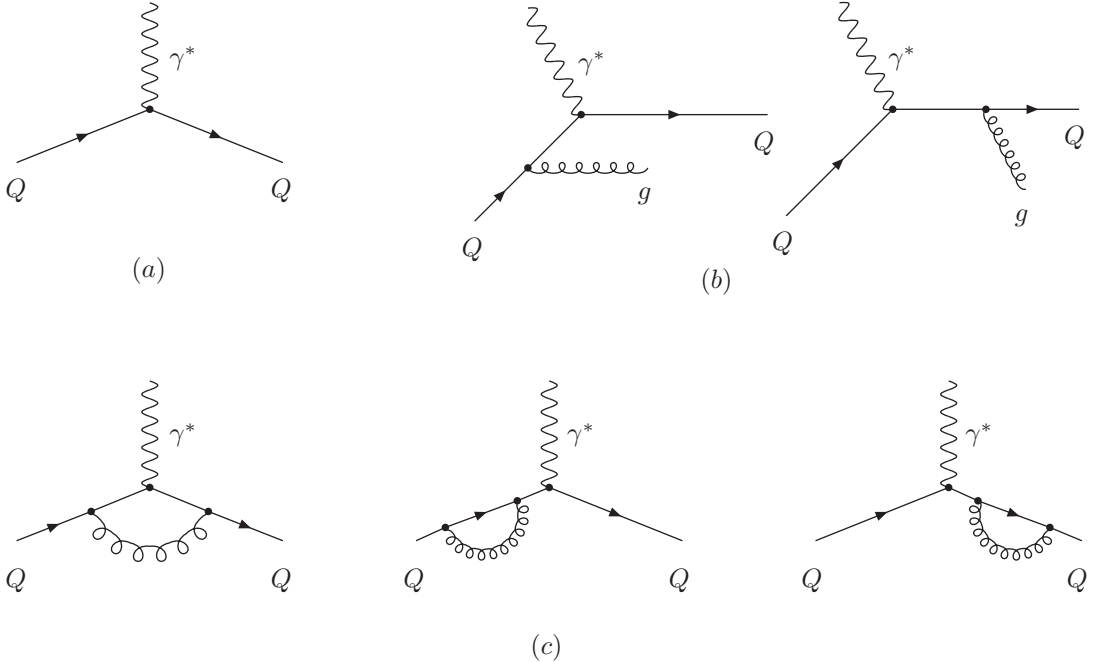


FIG. 2: The LO (a) and NLO (b and c) photon-quark scattering diagrams.

II. PARTONIC CROSS SECTIONS

A. Quark Scattering Mechanism

The momentum assignment of the deep inelastic lepton-quark scattering will be denoted as

$$l(\ell) + Q(k_Q) \rightarrow l(\ell - q) + Q(p_Q) + X(p_X). \quad (15)$$

Taking into account the target mass effects, the corresponding partonic cross section can be written as follows [30]

$$\frac{d^3\hat{\sigma}_{lQ}}{dz dQ^2 d\varphi} = \frac{\alpha_{em}}{(2\pi)^2} \frac{y^2}{zQ^2} \frac{\sqrt{1+4\lambda z^2}}{1-\hat{\varepsilon}} \left[\hat{\sigma}_{2,Q}(z, \lambda) - (1-\hat{\varepsilon})\hat{\sigma}_{L,Q}(z, \lambda) + \hat{\varepsilon}\hat{\sigma}_{A,Q}(z, \lambda) \cos 2\varphi + 2\sqrt{\hat{\varepsilon}(1+\hat{\varepsilon})}\hat{\sigma}_{I,Q}(z, \lambda) \cos \varphi \right]. \quad (16)$$

In Eq. (16), we use the following definition of partonic kinematic variables:

$$y = \frac{q \cdot k_Q}{\ell \cdot k_Q}, \quad z = \frac{Q^2}{2q \cdot k_Q}, \quad \lambda = \frac{m^2}{Q^2}. \quad (17)$$

In the massive case, the (virtual) photon polarization parameter, $\hat{\varepsilon}$, has the form [30]

$$\hat{\varepsilon} = \frac{2(1-y-\lambda z^2 y^2)}{1+(1-y)^2+2\lambda z^2 y^2}. \quad (18)$$

At leading order, $\mathcal{O}(\alpha_{em})$, the only quark scattering subprocess is

$$\gamma^*(q) + Q(k_Q) \rightarrow Q(p_Q). \quad (19)$$

The γ^*Q cross sections, $\hat{\sigma}_{k,Q}^{(0)}$ ($k = 2, L, A, I$), corresponding to the Born diagram (see Fig. 2a) are:

$$\begin{aligned} \hat{\sigma}_{2,Q}^{(0)}(z, \lambda) &= \hat{\sigma}_B(z) \sqrt{1+4\lambda z^2} \delta(1-z), \\ \hat{\sigma}_{L,Q}^{(0)}(z, \lambda) &= \hat{\sigma}_B(z) \frac{4\lambda z^2}{\sqrt{1+4\lambda z^2}} \delta(1-z), \\ \hat{\sigma}_{A,Q}^{(0)}(z, \lambda) &= \hat{\sigma}_{I,Q}^{(0)}(z, \lambda) = 0, \end{aligned} \quad (20)$$

with

$$\hat{\sigma}_B(z) = \frac{(2\pi)^2 e_Q^2 \alpha_{em}}{Q^2} z, \quad (21)$$

where e_Q is the quark charge in units of electromagnetic coupling constant.

To take into account the NLO $\mathcal{O}(\alpha_{em}\alpha_s)$ contributions, one needs to calculate the virtual corrections to the Born process (given in Fig. 2c) as well as the real gluon emission (see Fig. 2b):

$$\gamma^*(q) + Q(k_Q) \rightarrow Q(p_Q) + g(p_g). \quad (22)$$

The NLO φ -dependent cross sections, $\hat{\sigma}_{A,Q}^{(1)}$ and $\hat{\sigma}_{I,Q}^{(1)}$, are described by the real gluon emission only. Corresponding contributions are free of any type of singularities and the quantities $\hat{\sigma}_{A,Q}^{(1)}$ and $\hat{\sigma}_{I,Q}^{(1)}$ can be calculated directly in four dimensions.

In the φ -independent case, $\hat{\sigma}_{2,Q}^{(1)}$ and $\hat{\sigma}_{L,Q}^{(1)}$, we also work in four dimensions. The virtual contribution (Fig. 2c) contains ultraviolet (UV) singularity that is removed using the on-mass-shell regularization scheme. In particular, we calculate the absorptive part of the Feynman diagram which has no UV divergences. The real part is then obtained by using the appropriate dispersion relations. As to the infrared (IR) singularity, it is regularized with the help of an infinitesimal gluon mass. This IR divergence is cancelled when we add the bremsstrahlung contribution (Fig. 2b). Some details of our calculations are given in Appendix A.

The final (real+virtual) results for γ^*Q cross sections can be cast into the following form:

$$\begin{aligned} \hat{\sigma}_{2,Q}^{(1)}(z, \lambda) = & \frac{\alpha_s}{2\pi} C_F \hat{\sigma}_B(1) \sqrt{1+4\lambda} \delta(1-z) \left\{ -2 + 4 \ln \lambda - \sqrt{1+4\lambda} \ln r + \frac{1+2\lambda}{\sqrt{1+4\lambda}} \left[2\text{Li}_2(r^2) + 4\text{Li}_2(-r) \right. \right. \\ & \left. \left. + 3 \ln^2(r) - 4 \ln r + 4 \ln r \ln(1+4\lambda) - 2 \ln r \ln \lambda \right] \right\} \\ & + \frac{\alpha_s}{4\pi} C_F \hat{\sigma}_B(z) \frac{1}{(1+4\lambda z^2)^{3/2}} \left\{ \frac{1}{[1-(1-\lambda)z]^2} \left[1 - 3z - 4z^2 + 6z^3 + 8z^4 - 8z^5 \right. \right. \\ & \left. \left. + 6\lambda z (3 - 18z + 13z^2 + 10z^3 - 8z^4) \right. \right. \\ & \left. \left. + 4\lambda^2 z^2 (8 - 77z + 65z^2 - 2z^3) \right. \right. \\ & \left. \left. + 16\lambda^3 z^3 (1 - 21z + 12z^2) - 128\lambda^4 z^5 \right] \right\} \\ & + \frac{2 \ln D(z, \lambda)}{\sqrt{1+4\lambda z^2}} \left[- (1 + z + 2z^2 + 2z^3) + 2\lambda z (2 - 11z - 11z^2) + 8\lambda^2 z^2 (1 - 9z) \right] \\ & - \frac{8(1+4\lambda)^2 z^4}{(1-z)_+} - \frac{4(1+2\lambda)(1+4\lambda)^2 z^4 \ln D(z, \lambda)}{\sqrt{1+4\lambda z^2}} \frac{1}{(1-z)_+}, \end{aligned} \quad (23)$$

$$\begin{aligned} \hat{\sigma}_{L,Q}^{(1)}(z, \lambda) = & \frac{\alpha_s}{\pi} C_F \hat{\sigma}_B(1) \frac{2\lambda}{\sqrt{1+4\lambda}} \delta(1-z) \left\{ -2 + 4 \ln \lambda - \frac{4\lambda}{\sqrt{1+4\lambda}} \ln r + \frac{1+2\lambda}{\sqrt{1+4\lambda}} \left[2\text{Li}_2(r^2) + 4\text{Li}_2(-r) \right. \right. \\ & \left. \left. + 3 \ln^2(r) - 4 \ln r + 4 \ln r \ln(1+4\lambda) - 2 \ln r \ln \lambda \right] \right\} \\ & + \frac{\alpha_s}{\pi} C_F \hat{\sigma}_B(z) \frac{1}{(1+4\lambda z^2)^{3/2}} \left\{ \frac{z}{[1-(1-\lambda)z]^2} \left[(1-z)^2 - \lambda z (13 - 19z - 2z^2 + 8z^3) \right. \right. \\ & \left. \left. - 2\lambda^2 z^2 (31 - 39z + 8z^2) \right. \right. \\ & \left. \left. - 8\lambda^3 z^3 (10 - 7z) - 32\lambda^4 z^4 \right] \right. \\ & \left. - \frac{2\lambda z^2 \ln D(z, \lambda)}{\sqrt{1+4\lambda z^2}} [3 + 3z + 16\lambda z] \right. \\ & \left. - \frac{8\lambda(1+4\lambda)z^4}{(1-z)_+} - \frac{4\lambda(1+2\lambda)(1+4\lambda)z^4 \ln D(z, \lambda)}{\sqrt{1+4\lambda z^2}} \frac{1}{(1-z)_+} \right\}, \end{aligned} \quad (24)$$

$$\hat{\sigma}_{A,Q}^{(1)}(z, \lambda) = \frac{\alpha_s}{2\pi} C_F \hat{\sigma}_B(z) \frac{z(1-z)}{(1+4\lambda z^2)^{3/2}} \left\{ \frac{1}{[1-(1-\lambda)z]} [1 + 2\lambda(4 - 3z) + 8\lambda^2 z] + \frac{2\lambda \ln D(z, \lambda)}{\sqrt{1+4\lambda z^2}} [2 + z + 4\lambda z] \right\}, \quad (25)$$

$$\hat{\sigma}_{I,Q}^{(1)}(z, \lambda) = \frac{\alpha_s}{8\sqrt{2}} C_F \hat{\sigma}_B(z) \frac{1}{(1+4\lambda z^2)^2} \frac{\sqrt{z}}{[1-(1-\lambda)z]^{3/2}} \left\{ -(1-z)(1+2z) - 4\lambda z (10 - 10z - z^2 + 2z^3) \right. \\ \left. - 8\lambda^2 z^2 (25 - 29z + 8z^2) - 96\lambda^3 z^3 (3 - 2z) - 128\lambda^4 z^4 \right. \\ \left. + 8\sqrt{\lambda z [1-(1-\lambda)z]} [1-z^2 + \lambda z(13 - 11z) + 4\lambda^2 z^2(7 - 4z) + 16\lambda^3 z^3] \right\}. \quad (26)$$

In Eqs. (23-26), $C_F = (N_c^2 - 1)/(2N_c)$, where N_c is number of colors, while

$$D(z, \lambda) = \frac{1 + 2\lambda z - \sqrt{1 + 4\lambda z^2}}{1 + 2\lambda z + \sqrt{1 + 4\lambda z^2}}, \quad r = \sqrt{D(z=1, \lambda)} = \frac{\sqrt{1 + 4\lambda} - 1}{\sqrt{1 + 4\lambda} + 1}. \quad (27)$$

The so-called "plus" distributions are defined by

$$[g(z)]_+ = g(z) - \delta(1-z) \int_0^1 d\zeta g(\zeta). \quad (28)$$

For any sufficiently regular test function $h(z)$, Eq. (28) gives

$$\int_a^1 dz h(z) \left[\frac{\ln^k(1-z)}{1-z} \right]_+ = \int_a^1 dz \frac{\ln^k(1-z)}{1-z} [h(z) - h(1)] + h(1) \frac{\ln^{k+1}(1-a)}{k+1}. \quad (29)$$

To perform a numerical investigation of the inclusive partonic cross sections, $\hat{\sigma}_{k,Q}$ ($k = T, L, A, I$), it is convenient to introduce the dimensionless coefficient functions $c_{k,Q}^{(n,l)}$,

$$\hat{\sigma}_{k,Q}(\eta, \lambda, \mu^2) = \frac{e_Q^2 \alpha_{em} \alpha_s(\mu^2)}{m^2} \sum_{n=0}^{\infty} (4\pi \alpha_s(\mu^2))^n \sum_{l=0}^n c_{k,Q}^{(n,l)}(\eta, \lambda) \ln^l \left(\frac{\mu^2}{m^2} \right), \quad (30)$$

where μ is a factorization scale (we use $\mu = \mu_F = \mu_R$) and the variable η measures the distance to the partonic threshold:

$$\eta = \frac{s}{m^2} - 1 = \frac{1-z}{\lambda z}, \quad s = (q+k_Q)^2. \quad (31)$$

Our analysis of the quantity $c_{A,Q}^{(0,0)}(\eta, \lambda)$ is given in Fig. 3. One can see that $c_{A,Q}^{(0,0)}$ is negative at low Q^2 ($\lambda^{-1} \lesssim 1$) and positive at high Q^2 ($\lambda^{-1} > 20$). For the intermediate values of Q^2 , $c_{A,Q}^{(0,0)}(\eta, \lambda)$ is an alternating function of η .

Our results for the coefficient function $c_{I,Q}^{(0,0)}(\eta, \lambda)$ at several values of λ are presented in Fig. 3. It is seen that $c_{I,Q}^{(0,0)}$ is negative at all values of η and λ . Note also the threshold behavior of the coefficient function:

$$c_{I,Q}^{(0,0)}(\eta \rightarrow 0, \lambda) = -\sqrt{2}\pi^2 C_F \frac{\sqrt{\lambda}}{1+4\lambda} + \mathcal{O}(\eta). \quad (32)$$

This quantity takes its minimum value at $\lambda_m = 1/4$: $c_{I,Q}^{(0,0)}(\eta=0, \lambda_m) = -\pi^2 C_F / (2\sqrt{2})$.

B. Comparison with Available Results

For the first time, the NLO $\mathcal{O}(\alpha_{em} \alpha_s)$ corrections to the φ -independent IC contribution have been calculated a long time ago by Hoffmann and Moore (HM) [25]. However, authors of Ref. [25] don't give explicitly their definition of the partonic cross sections that leads to a confusion in interpretation of the original HM results. To clarify the situation, we need first to derive the relation between the lepton-quark DIS cross section, $d\hat{\sigma}_{lQ}$, and the partonic cross sections, $\sigma^{(2)}$ and $\sigma^{(L)}$, used in [25]. Using Eqs. (C.1) and (C.5) in Ref. [25], one can express the HM tensor $\sigma_R^{\mu\nu}$ in terms of "our" cross sections $\hat{\sigma}_{2,Q}$ and $\hat{\sigma}_{L,Q}$ defined by Eq. (16) in the present paper. Comparing the obtained results

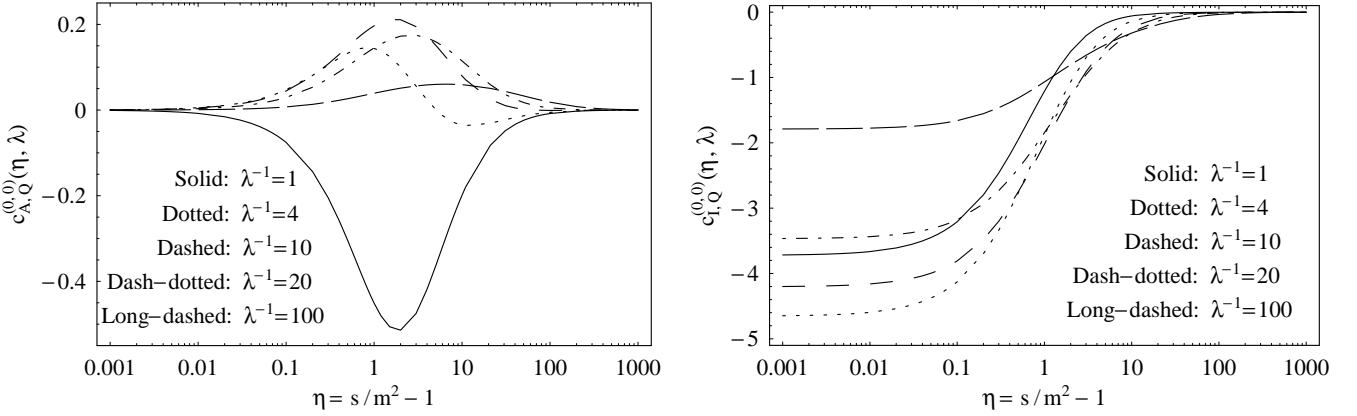


FIG. 3: $c_{A,Q}^{(0,0)}(\eta, \lambda)$ and $c_{I,Q}^{(0,0)}(\eta, \lambda)$ coefficient functions at several values of λ .

with the corresponding definition of $\sigma_R^{\mu\nu}$ via the HM cross sections $\sigma^{(2)}$ and $\sigma^{(L)}$ (given by Eqs. (C.16) and (C.17) in Ref. [25]), we find that

$$\hat{\sigma}_{2,Q}(z, \lambda) \equiv \hat{\sigma}_B(z) \sqrt{1 + 4\lambda z^2} \sigma^{(2)}(z, \lambda), \quad (33)$$

$$\hat{\sigma}_{L,Q}(z, \lambda) \equiv \frac{2\hat{\sigma}_B(z)}{\sqrt{1 + 4\lambda z^2}} [\sigma^{(L)}(z, \lambda) + 2\lambda z^2 \sigma^{(2)}(z, \lambda)]. \quad (34)$$

Now we are able to compare our results with original HM ones. It is easy to see that the LO cross sections (defined by Eqs. (37) in [25] and Eqs. (20) in our paper) obey both above identities. Comparing with each other the quantities $\sigma_1^{(2)}$ and $\hat{\sigma}_{2,Q}^{(1)}$ (given by Eq. (51) in [25] and Eq. (23) in this paper, respectively), we find that identity (33) is satisfied at NLO too. The situation with longitudinal cross sections is more complicated. We have uncovered two misprints in the NLO expression for $\sigma^{(L)}$ given by Eq. (52) in [25]. First, the r.h.s. of this Eq. must be multiplied by z . Second, the sign in front of the last term (proportional to $\delta(1-z)$) in Eq. (52) in Ref. [25] must be changed². Taking into account these typos, we find that relation (34) holds at NLO as well. So, our calculations of $\hat{\sigma}_{2,Q}$ and $\hat{\sigma}_{L,Q}$ agree with the HM results.

Recently, the heavy quark initiated contributions to the φ -independent DIS structure functions, F_2 and F_L , have been calculated by Kretzer and Schienbein (KS) [26]. The final KS results are expressed in terms of the parton level structure functions \hat{H}_1^q and \hat{H}_2^q . Using the definition of \hat{H}_1^q and \hat{H}_2^q given by Eqs. (7, 8) in Ref. [26], we obtain that

$$\hat{\sigma}_{T,Q}(z, \lambda) \equiv \frac{\alpha_s}{2\pi} \frac{\hat{\sigma}_B(z)}{\sqrt{1 + 4\lambda}} \frac{\hat{H}_1^q(\xi', \lambda)}{\sqrt{1 + 4\lambda z^2}}, \quad \hat{\sigma}_{2,Q}(z, \lambda) \equiv \frac{\alpha_s}{2\pi} \hat{\sigma}_B(z) \sqrt{\frac{1 + 4\lambda}{1 + 4\lambda z^2}} \hat{H}_2^q(\xi', \lambda), \quad (35)$$

where $\hat{\sigma}_{T,Q} = \hat{\sigma}_{2,Q} - \hat{\sigma}_{L,Q}$ and $\hat{\sigma}_{L,Q}$ are defined by Eq. (16) in our paper and $\xi' = z(1 + \sqrt{1 + 4\lambda}) / (1 + \sqrt{1 + 4\lambda z^2})$. To test identities (35), one needs only to rewrite the NLO expressions for the functions $\hat{H}_1^q(\xi', \lambda)$ and $\hat{H}_2^q(\xi', \lambda)$ (given in Appendix C in Ref. [26]) in terms of variables z and λ . Our analysis shows that relations (35) hold at both LO and NLO. Hence we coincide with the KS predictions for the γ^*Q cross sections.

However, we disagree with the conclusion of Ref. [26] that there are errors in the NLO expression for $\sigma^{(2)}$ given in Ref. [25]³. As explained above, a correct interpretation of the quantities $\sigma^{(2)}$ and $\sigma^{(L)}$ used in [25] leads to a complete agreement between the HM, KS and our results for φ -independent cross sections.

As to the φ -dependent DIS, pQCD predictions for the γ^*Q cross sections $\hat{\sigma}_{A,Q}(z, \lambda)$ and $\hat{\sigma}_{I,Q}(z, \lambda)$ in the case of arbitrary values of m^2 and Q^2 are not, to our knowledge, available in the literature. For this reason, we have performed several cross checks of our results against well known calculations in two limits: $m^2 \rightarrow 0$ and $Q^2 \rightarrow 0$. In particular, in the chiral limit, we reproduce the original results of Georgi and Politzer [32] and Méndez [33] for

² Note that this term originates from virtual corrections and the virtual part of the longitudinal cross section given by Eq. (39) in Ref. [25] also has wrong sign. See Appendix A for more details.

³ In detail, the KS point of view on the HM results is presented in PhD thesis [31], pp. 158-160.

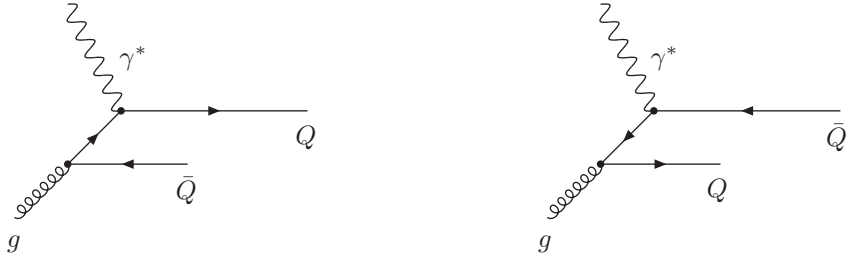


FIG. 4: The LO photon-gluon fusion diagrams.

$\hat{\sigma}_{I,Q}(z, \lambda \rightarrow 0)$ and $\hat{\sigma}_{A,Q}(z, \lambda \rightarrow 0)$. In the case of $Q^2 \rightarrow 0$, our predictions for $\hat{\sigma}_{2,Q}(s, Q^2 \rightarrow 0)$ and $\hat{\sigma}_{A,Q}(s, Q^2 \rightarrow 0)$ given by Eqs. (23,25) reduce to the QED textbook results for the Compton scattering of polarized photons [34].

C. Photon-Gluon Fusion

The gluon fusion component of the semi-inclusive DIS is the following parton level interaction:

$$l(\ell) + g(k_g) \rightarrow l(\ell - q) + Q(p_Q) + X[\bar{Q}](p_{\bar{Q}}). \quad (36)$$

Corresponding lepton-gluon cross section, $d\hat{\sigma}_{lg}$, has the following decomposition in terms of the helicity $\gamma^* g$ cross sections:

$$\frac{d^3\hat{\sigma}_{lg}}{dz dQ^2 d\varphi} = \frac{\alpha_{em}}{(2\pi)^2} \frac{1}{zQ^2} \frac{y^2}{1-\varepsilon} \left[\hat{\sigma}_{2,g}(z, \lambda) - (1-\varepsilon)\hat{\sigma}_{L,g}(z, \lambda) + \varepsilon\hat{\sigma}_{A,g}(z, \lambda) \cos 2\varphi + 2\sqrt{\varepsilon(1+\varepsilon)}\hat{\sigma}_{I,g}(z, \lambda) \cos \varphi \right], \quad (37)$$

where the quantity ε is defined by Eq. (3) with $y = (q \cdot k_g) / (\ell \cdot k_g)$.

At LO, $\mathcal{O}(\alpha_{em}\alpha_s)$, the only gluon fusion subprocess responsible for heavy flavor production is

$$\gamma^*(q) + g(k_g) \rightarrow Q(p_Q) + \bar{Q}(p_{\bar{Q}}). \quad (38)$$

The $\gamma^* g$ cross sections, $\hat{\sigma}_{k,g}^{(0)}$ ($k = 2, L, A, I$), corresponding to the Born diagrams given in Fig. 4 have the form [35, 36]:

$$\begin{aligned} \hat{\sigma}_{2,g}^{(0)}(z, \lambda) &= \frac{\alpha_s}{2\pi} \hat{\sigma}_B(z) \left\{ [(1-z)^2 + z^2 + 4\lambda z(1-3z) - 8\lambda^2 z^2] \ln \frac{1+\beta_z}{1-\beta_z} - [1+4z(1-z)(\lambda-2)] \beta_z \right\}, \\ \hat{\sigma}_{L,g}^{(0)}(z, \lambda) &= \frac{2\alpha_s}{\pi} \hat{\sigma}_B(z) z \left\{ -2\lambda z \ln \frac{1+\beta_z}{1-\beta_z} + (1-z) \beta_z \right\}, \\ \hat{\sigma}_{A,g}^{(0)}(z, \lambda) &= \frac{\alpha_s}{\pi} \hat{\sigma}_B(z) z \left\{ 2\lambda [1-2z(1+\lambda)] \ln \frac{1+\beta_z}{1-\beta_z} + (1-2\lambda)(1-z) \beta_z \right\}, \\ \hat{\sigma}_{I,g}^{(0)}(z, \lambda) &= 0, \end{aligned} \quad (39)$$

where $\hat{\sigma}_B(z)$ is defined by Eq. (21) and the following notations are used:

$$z = \frac{Q^2}{2q \cdot k_g}, \quad \lambda = \frac{m^2}{Q^2}, \quad \beta_z = \sqrt{1 - \frac{4\lambda z}{1-z}}. \quad (40)$$

Note that the $\cos \varphi$ dependence vanishes in the GF mechanism due to the $Q \leftrightarrow \bar{Q}$ symmetry which, at leading order, requires invariance under $\varphi \rightarrow \varphi + \pi$ [37].

As to the NLO results, presently, only φ -independent quantities $\hat{\sigma}_{2,g}^{(1)}$ and $\hat{\sigma}_{L,g}^{(1)}$ are known exactly [38]. For this reason, we will use in our analysis the so-called soft-gluon approximation for the NLO $\gamma^* g$ cross sections (see Appendix B). As shown in Refs. [20, 21, 39], at energies not so far from the production threshold, the soft-gluon radiation is the dominant perturbative mechanism in the $\gamma^* g$ interactions.

III. HADRON LEVEL RESULTS

A. Fixed Flavor Number Scheme and Nonperturbative Intrinsic Charm

In the fixed flavor number scheme⁴, the wave function of the proton consists of light quarks u, d, s and gluons g . Heavy flavor production in DIS is dominated by the gluon fusion mechanism. Corresponding hadron level cross sections, $\sigma_{k,GF}(x, \lambda)$, have the form

$$\sigma_{k,GF}(x, \lambda) = \int_{\chi}^1 dz g(z, \mu_F) \hat{\sigma}_{k,g}(x/z, \lambda, \mu_F), \quad (k = 2, L, A, I), \quad (41)$$

$$\chi = x(1 + 4\lambda), \quad (42)$$

where $g(z, \mu_F)$ describes gluon density in the proton evaluated at a factorization scale μ_F . The lowest order GF cross sections, $\hat{\sigma}_{k,g}^{(0)}$ ($k = 2, L, A, I$), are given by Eqs. (39). The NLO results, $\hat{\sigma}_{k,g}^{(1)}$, to the next-to-leading logarithmic accuracy are presented in Appendix B.

We neglect the $\gamma^* q(\bar{q})$ fusion subprocesses. This is justified as their contributions to heavy quark lepto-production vanish at LO and are small at NLO [38].

In the FFNS, the intrinsic heavy flavor component of the proton wave function is generated by $gg \rightarrow Q\bar{Q}$ fluctuations where the gluons are coupled to different valence quarks. In the present paper, this component is referred to as the nonperturbative intrinsic charm (bottom). The probability of the corresponding five-quark Fock state, $|uudQ\bar{Q}\rangle$, is of higher twist since it scales as Λ_{QCD}^2/m^2 [5]. However, since all of the quarks tend to travel coherently at same rapidity in the $|uudQ\bar{Q}\rangle$ bound state, the heaviest constituents carry the largest momentum fraction. For this reason, the heavy flavor distribution function has a more "hard" z -behavior than the light parton densities. Since all of the densities vanish at $z \rightarrow 1$, the hardest PDF becomes dominant at sufficiently large z independently of normalization.

Convolution of PDFs with partonic cross sections does not violate this observation. In particular, assuming a gluon density $g(z) \sim (1 - z)^n$ (where $n = 3 - 5$), we obtain that the LO GF contribution to F_2 scales as $(1 - \chi)^{n+3/2}$ at $\chi \rightarrow 1$, where χ is defined by Eq. (42). In the case of Hoffman and Moore charm density (see below), the LO IC contribution is proportional to $(1 - \chi)$ at $\chi \rightarrow 1$. It is easy to see that, independently of normalizations, the IC contribution to be dominate over the more "soft" GF component at large enough x .

For the first time, the intrinsic charm momentum distribution in the five-quark state $|uudcc\bar{c}\rangle$ was derived by Brodsky, Hoyer, Peterson and Sakai (BHPS) in the framework of a light-cone model [1, 2]. Neglecting the transverse motion of constituents, they have obtained in the heavy quark limit that

$$c(z) = \frac{N_5}{6} z^2 [6z(1 + z) \ln z + (1 - z)(1 + 10z + z^2)], \quad (43)$$

where $N_5 = 36$ corresponds to a 1% probability for IC in the nucleon: $\int_0^1 c(z) dz = 0.01$.

Hoffmann and Moore (HM) [25] incorporated mass effects in the BHPS approach. They first introduced a mass scaling variable ξ ,

$$\xi = \frac{2ax}{1 + \sqrt{1 + 4\lambda_N x^2}}, \quad a = \frac{1 + \sqrt{1 + 4\lambda}}{2}, \quad (44)$$

where $\lambda_N = m_N^2/Q^2$. To provide correct threshold behavior of the charm density, the constraint $\xi \leq \gamma < 1$ was imposed where

$$\gamma = \frac{2a\hat{x}}{1 + \sqrt{1 + 4\lambda_N \hat{x}^2}}, \quad \hat{x} = \frac{1}{1 + 4\lambda - \lambda_N}. \quad (45)$$

Resulting charm distribution function, $c(\xi, \gamma)$, has the following form in the HM approach:

$$c(\xi, \gamma) = \begin{cases} c(\xi) - \frac{\xi}{\gamma} c(\gamma), & \xi \leq \gamma \\ 0, & \xi > \gamma \end{cases} \quad (46)$$

⁴ This approach is sometimes referred to as the fixed-order perturbation theory (FOPT).

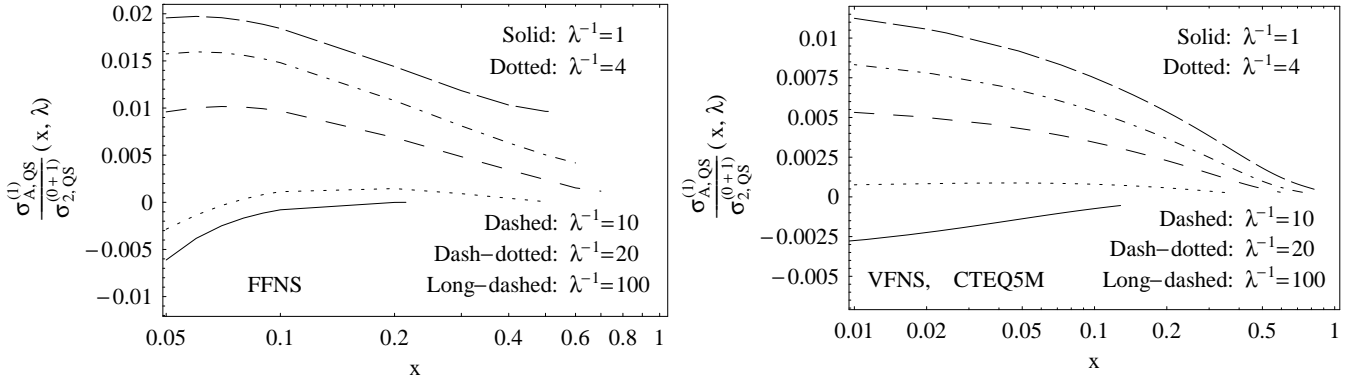


FIG. 5: The quantity $(\sigma_{A,QS}^{(1)} / \sigma_{2,QS}^{(0+1)})(x, \lambda)$ in the FFNS with the HM [25] charm density (*left panel*) and in the VFNS with the CTEQ5M charm distribution function (*right panel*).

with $c(\xi)$ defined by Eq. (43). Corresponding hadron level cross sections for the $(c + \bar{c})$ production, $\sigma_{k,QS}(x, \lambda)$, due to the heavy quark scattering (QS) mechanism, are

$$\sigma_{k,QS}(x, \lambda) = \int_{\xi}^{\gamma} \frac{dz}{\sqrt{1 + 4\lambda\xi^2/z^2}} c_+(z, \gamma) \hat{\sigma}_{k,c}(\xi/z, \lambda), \quad (k = 2, L, A, I), \quad (47)$$

where the charm density $c_+(z, \gamma) \equiv c(z, \gamma) + \bar{c}(z, \gamma)$. The LO and NLO expressions for the partonic cross sections $\hat{\sigma}_{k,c}(z, \lambda)$ are given by Eqs. (20) and (23-26), respectively.

Note also that, in the FFNS, the full cross section for the charm production, $\sigma_k(x, \lambda)$, is simply a sum of the GF and IC components:

$$\sigma_k(x, \lambda) = \sigma_{k,GF}(x, \lambda) + \sigma_{k,QS}(x, \lambda), \quad (k = 2, L, A, I), \quad (48)$$

Let us discuss the FFNS predictions for the hadron level asymmetry parameter $A(x, Q^2)$ defined by Eq. (11). First we consider the ratio $(\sigma_{A,QS}^{(1)} / \sigma_{2,QS}^{(0+1)})(x, \lambda)$, i.e., the mere IC contribution to $A(x, Q^2)$. In Fig. 5, the x -behavior of this quantity at various values of λ is presented. One can see that the ratio $(\sigma_{A,QS}^{(1)} / \sigma_{2,QS}^{(0+1)})(x, \lambda)$ is negligibly small (of the order of 1%) practically at all values of $Q^2 > m^2$. Note that this fact is independent of the charm density we use (see, for instance, the right panel in Fig. 5), but is only due to the smallness of the partonic cross section $\hat{\sigma}_{A,c}^{(1)}(z, \lambda)$ [30]. So, the quantity $\sigma_{A,QS}(x, \lambda)$ is exactly zero at LO⁵ and negligibly small at NLO. This implies that the IC contribution has no practically $\cos 2\varphi$ -dependence and, for this reason, we will neglect both $\hat{\sigma}_{A,c}(z, \lambda)$ and $\sigma_{A,QS}(x, \lambda)$ cross sections in our further analysis.

Fig. 6 shows $A(x, \lambda)$ as a function of x for several values of variable λ : $\lambda^{-1} = 1, 4, 10, 20, 50$ and 100 . We display both LO and NLO predictions of the GF mechanism as well as the analogous results of the combined GF+QS contribution. The azimuthal asymmetry due to the mere LO GF component is given by solid line. The NLO GF predictions are plotted by dashed line. The LO and NLO results of the total GF+QS contribution are given by dash-dotted and long-dashed lines, respectively. In our calculations, the CTEQ5M [40] parametrization of the gluon distribution function is used and a 1% probability for IC in the nucleon is assumed. Throughout this paper, the value $\mu_F = \mu_R = \sqrt{m^2 + Q^2}$ for both factorization and renormalization scales is chosen. In accordance with the CTEQ5M parametrization, we use $m_c = 1.3$ GeV and $\Lambda_4 = 326$ MeV [40].

One can see from Fig. 6 the following basic features of the azimuthal asymmetry, $A(x, \lambda)$, within the FFNS. First, as expected, the nonperturbative IC contribution is practically invisible at low x , but affects essentially the GF predictions at large x . Since, contrary to the GF mechanism, the QS component is practically $\cos 2\varphi$ -independent,

⁵ Remember that the LO quantity $\hat{\sigma}_{A,c}^{(0)}(z, \lambda)$ vanishes for the kinematic reason, see Eqs. (20).

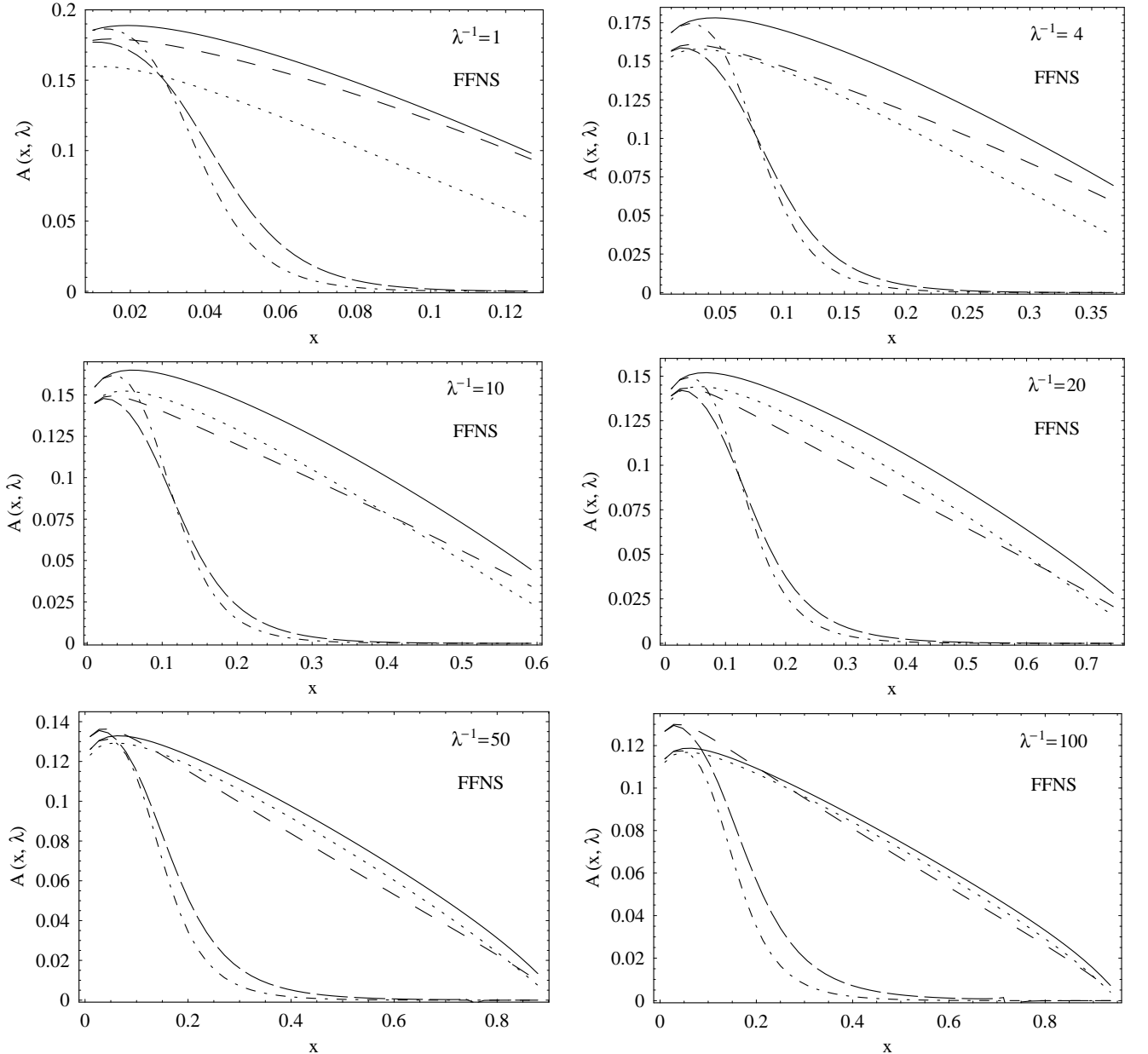


FIG. 6: Azimuthal asymmetry parameter $A(x, \lambda)$ in the FFNS at several values of λ in the case of $\int_0^1 c(z) dz = 1\%$. The following contributions are plotted: $GF^{(LO)}$ (solid lines), $GF^{(LO)} + k_T\text{-kick}$ (dotted lines), $GF^{(NLO)}$ (dashed lines), $GF^{(LO)} + QS^{(LO)}$ (dash-dotted lines) and $GF^{(NLO)} + QS^{(NLO)}$ (long-dashed lines).

the dominance of the IC contribution at large x leads to a more rapid (in comparison with the GF predictions) decreasing of $A(x, \lambda)$ with growth of x .

The most remarkable property of the azimuthal asymmetry is its perturbative stability. In Refs. [20, 21], the NLO soft-gluon corrections to the GF predictions for the $\cos 2\varphi$ asymmetry in heavy quark photo- and lepto-production was calculated. It was shown that, contrary to the production cross sections, the quantity $A(x, \lambda)$ is practically insensitive to soft radiation. One can see from Fig. 6 in the present paper that the NLO corrections to the LO GF predictions for $A(x, \lambda)$ are about few percent at not large x . This implies that large soft-gluon corrections to $\sigma_{A,GF}^{(LO)}$ and $\sigma_{2,GF}^{(LO)}$ (increasing both cross sections by a factor of two) cancel each other in the ratio $(\sigma_{A,GF}^{(NLO)} / \sigma_{2,GF}^{(NLO)})(x, \lambda)$ with a good accuracy. In terms of so-called K -factors, $K_k(x, \lambda) = (\sigma_k^{(NLO)} / \sigma_k^{(LO)})(x, \lambda)$ for $k = 2, L, A, I$, perturbative stability of

the GF predictions for $A(x, \lambda)$ is provided by the fact that the corresponding K -factors are approximately the same at not large x : $K_{A,GF}(x, \lambda) \approx K_{2,GF}(x, \lambda)$.

Comparing with each other the dash-dotted and long-dashed curves in Fig. 6, we see that the NLO corrections to the combined GF+QS result for $A(x, \lambda)$ are also small. In this case, three reasons are responsible for the closeness of the LO and NLO predictions. At small x , where the nonperturbative IC contribution is negligible, perturbative stability of the asymmetry is provided by the GF component. In the large- x region, where the IC mechanism dominates, the azimuthal asymmetry rapidly vanishes with growth of x at both LO and NLO because the QS component is practically $\cos 2\varphi$ -independent, $\hat{\sigma}_{A,c}^{(1)}(x, \lambda) \approx \hat{\sigma}_{A,c}^{(0)}(x, \lambda) = 0$ ⁶. At intermediate values of x , where both mechanisms are essential, perturbative stability of $A(x, \lambda)$ is due to the similarity of the corresponding K -factors: $K_{2,GF}(x, \lambda) \sim K_{2,QS}(x, \lambda)$ ⁷.

Another remarkable property of the azimuthal asymmetry closely related to fast perturbative convergence is its parametric stability⁸. The analysis of Refs. [19, 21] shows that the GF predictions for the $\cos 2\varphi$ asymmetry are less sensitive to standard uncertainties in the QCD input parameters ($m, \mu_R, \mu_F, \Lambda_{QCD}$ and PDFs) than the corresponding ones for the production cross sections. We have verified that the same situation takes also place for the combined GF+QS results.

Let us discuss how the GF predictions for the azimuthal asymmetry are affected by nonperturbative contributions due to the intrinsic transverse motion of the gluon in the target. Because of the relatively low c -quark mass, these contributions are especially important in the description of the cross sections for charmed particle production.

To introduce k_T degrees of freedom, $\vec{k}_g \simeq \zeta \vec{p} + \vec{k}_T$, one extends the integral over the parton distribution function in Eq. (41) to k_T -space,

$$d\zeta g(\zeta, \mu_F) \rightarrow d\zeta d^2 k_T f(\vec{k}_T) g(\zeta, \mu_F). \quad (49)$$

The transverse momentum distribution, $f(\vec{k}_T)$, is usually taken to be a Gaussian:

$$f(\vec{k}_T) = \frac{e^{-\vec{k}_T^2/\langle k_T^2 \rangle}}{\pi \langle k_T^2 \rangle}. \quad (50)$$

In practice, an analytic treatment of k_T effects is usually used. According to Ref. [41], the k_T -smeared differential cross section of the process (1) is a two-dimensional convolution:

$$\frac{d^4 \sigma_{IN}^{\text{kick}}}{dx dQ^2 dp_{QT} d\varphi}(\vec{p}_{QT}) = \int d^2 k_T \frac{e^{-\vec{k}_T^2/\langle k_T^2 \rangle}}{\pi \langle k_T^2 \rangle} \frac{d^4 \sigma_{IN}}{dx dQ^2 dp_{QT} d\varphi} \left(\vec{p}_{QT} - \frac{1}{2} \vec{k}_T \right). \quad (51)$$

The factor $\frac{1}{2}$ in front of \vec{k}_T in the r.h.s. of Eq. (51) reflects the fact that the heavy quark carries away about one half of the initial energy in the reaction (1).

Values of the k_T -kick corrections to the LO GF predictions for the $\cos 2\varphi$ asymmetry in the charm production are shown in Fig. 6 by dotted curves. Calculating the k_T -kick effect we use $\langle k_T^2 \rangle = 0.5 \text{ GeV}^2$. One can see that k_T -smearing for $A(x, Q^2)$ is about 20-25% in the region of low $Q^2 \lesssim m^2$ and rapidly decreases at high Q^2 .

In Fig. 7, the dependence of the asymmetry $A(x, \lambda)$ on the nonperturbative intrinsic charm content of the proton is presented. We plot the LO predictions for $A(x, \lambda)$ as a function of x for several values of the variable λ and quantity $P_c = \int_0^1 c(z) dz$ describing a probability for IC in the nucleon. Dash-dotted curves describe the $\text{GF}^{(\text{LO})} + \text{QS}^{(\text{LO})}$ contributions with $P_c = 5\%, 1\%, 0.1\%$ and 0.01% . Solid lines correspond to the case when $P_c = 0$. Comparing with each other Figs. 6 and 7, one can see that even a 0.1% contribution of the nonperturbative IC to the proton wave function could be extracted from the $\cos 2\varphi$ asymmetry at large enough Bjorken x .

B. Variable Flavor Number Scheme and Perturbative Intrinsic Charm

One can see from Eqs. (39) that the GF cross section $\hat{\sigma}_{2,g}^{(0)}(z, \lambda)$ contains potentially large logarithm, $\ln(Q^2/m^2)$. The same situation takes also place for the QS cross section $\hat{\sigma}_{2,Q}^{(1)}(z, \lambda)$ given by Eq. (23). At high energies, $Q^2 \rightarrow$

⁶ Although the ratio $(A^{(\text{NLO})}/A^{(\text{LO})})(x, \lambda)$ is sizeable at sufficiently large x , the absolute values of the quantities $A^{(\text{LO})}(x, \lambda)$ and $A^{(\text{NLO})}(x, \lambda)$ become so small that it seems reasonable to consider the asymmetry as equally negligible at both LO and NLO and treat the predictions as perturbatively stable.

⁷ Note however that this similarity takes only place at intermediate values of x where both GF and QS components are essential. In the low- and large- x regions, the factors $K_{2,GF}(x, \lambda)$ and $K_{2,QS}(x, \lambda)$ are strongly different.

⁸ Of course, parametric stability of the fixed order results does not imply a fast convergence of the corresponding series. However, a fast convergent series must be parametrically stable. In particular, it must be μ_R - and μ_F -independent.

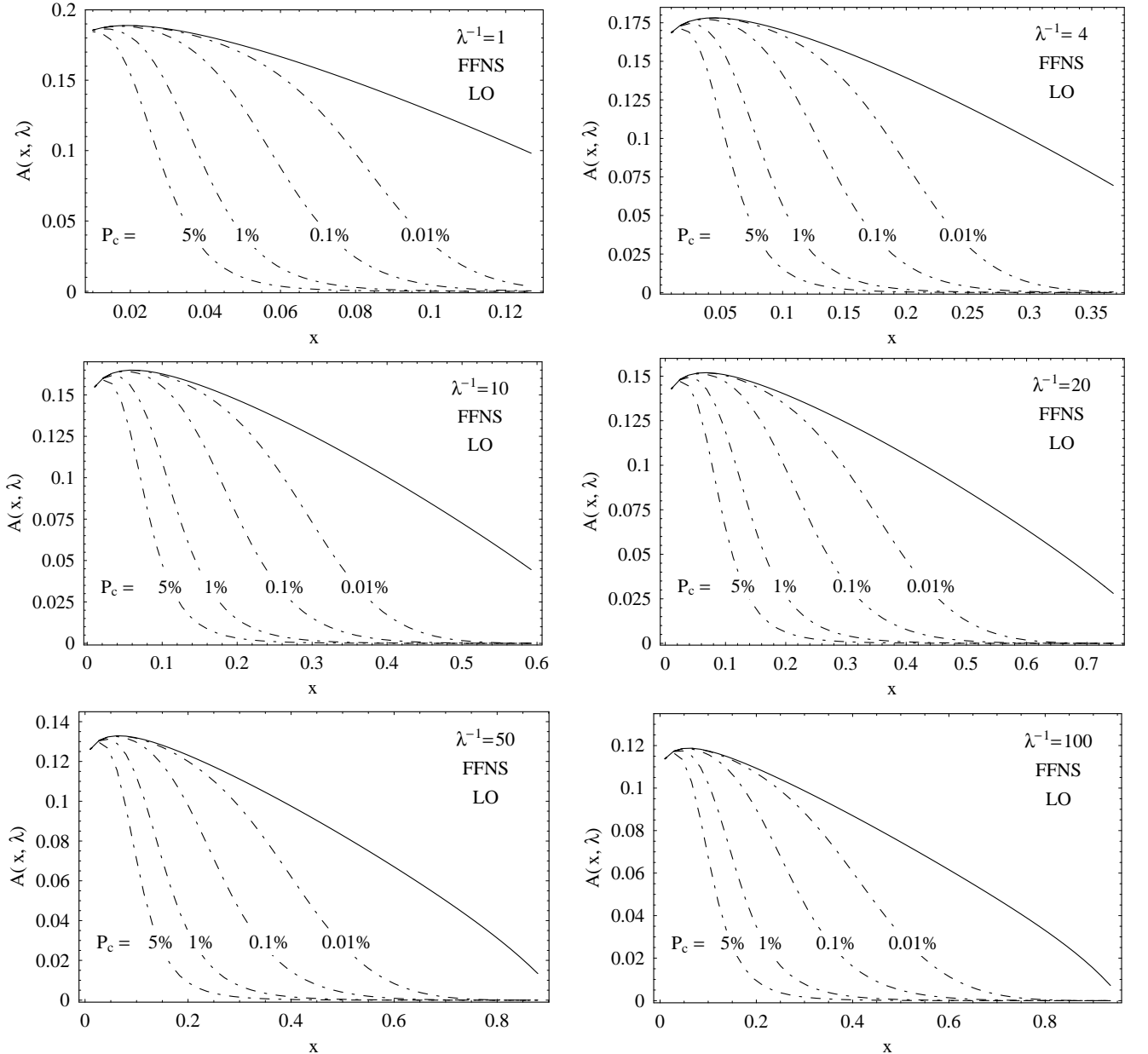


FIG. 7: The LO predictions for $A(x, \lambda)$ in the FFNS at several values of λ and $P_c = \int_0^1 c(z) dz$. Dash-dotted curves describe the $GF^{(LO)} + QS^{(LO)}$ contributions with $P_c = 5\%, 1\%, 0.1\%$ and 0.01% . Solid lines correspond to the case when $P_c = 0$.

∞ , the terms of the form $\alpha_s^n \ln(Q^2/m^2)$ dominate the production cross sections. To improve the convergence of the perturbative series at high energies, the so-called variable flavor number schemes (VFNS) have been proposed. Originally, this approach was formulated by Aivazis, Collins, Olness and Tung (ACOT) [6, 42].

In the VFNS, the mass logarithms of the type $\alpha_s^n \ln^n(Q^2/m^2)$ are resummed via the renormalization group equations. In practice, the resummation procedure consists of two steps. First, the mass logarithms have to be subtracted from the fixed order predictions for the partonic cross sections in such a way that in the asymptotic limit $Q^2 \rightarrow \infty$ the well known massless \overline{MS} coefficient functions are recovered. Instead, a charm parton density in the hadron, $c(x, Q^2)$, has to be introduced. This density obeys the usual massless NLO DGLAP evolution equation with the boundary condition $c(x, Q^2 = Q_0^2) = 0$ where $Q_0^2 \sim m^2$. So, we may say that, within the VFNS, the charm density arises perturbatively from the $g \rightarrow c\bar{c}$ evolution.

In the VFNS, the treatment of the charm depends on the values chosen for Q^2 . At low $Q^2 < Q_0^2$, the production

cross sections are described by the light parton contributions (u, d, s and g). The charm production is dominated by the GF process and its higher order QCD corrections. At high $Q^2 \gg m^2$, the charm is treated in the same way as the other light quarks and it is represented by a charm parton density in the hadron, which evolves in Q^2 . In the intermediate scale region, $Q^2 \sim m^2$, one has to make a smooth connection between the two different prescriptions.

Strictly speaking, the perturbative charm density is well defined at high $Q^2 \gg m^2$ but does not have a clean interpretation at low Q^2 . Since the perturbative IC originates from resummation of the mass logarithms of the type $\alpha_s^n \ln^n(Q^2/m^2)$, it is usually assumed that the corresponding PDF vanishes with these logarithms, i.e. for $Q^2 < Q_0^2 \approx m^2$. On the other hand, the threshold constraint $W^2 = (q+p)^2 = Q^2(1/x - 1) > 4m^2$ implies that Q_0 is not a constant but "live" function of x . To avoid this problem, several solutions have been proposed (see e.g. Refs. [43, 45]). In this paper, we use the so-called ACOT(χ) prescription [43] which guarantees (at least at $Q^2 > m^2$) the correct threshold behavior of the heavy-quark-initiated contributions.

Within the VFNS, the φ -independent charm production cross sections have three pieces:

$$\sigma_2(x, \lambda) = \sigma_{2,GF}(x, \lambda) - \sigma_{2,SUB}(x, \lambda) + \sigma_{2,QS}(x, \lambda), \quad (52)$$

where the first and third terms on the right hand side describe the usual (unsubtracted) GF and QS contributions while the second (subtraction) term renders the total result infra-red safe in the limit $m^2 \rightarrow 0$. The only constraint imposed on the subtraction term is to reproduce at high energies the familiar $\overline{\text{MS}}$ partonic cross section:

$$\lim_{\lambda \rightarrow 0} [\hat{\sigma}_{2,g}(z, \lambda) - \hat{\sigma}_{2,SUB}(z, \lambda)] = \hat{\sigma}_{2,g}^{\overline{\text{MS}}}(z). \quad (53)$$

Evidently, there is some freedom in the choice of finite mass terms of the form λ^n (with a positive n) in $\hat{\sigma}_{2,SUB}(z, \lambda)$. For this reason, several prescriptions have been proposed to fix the subtraction term. As mentioned above, we use the so-called ACOT(χ) scheme [43].

According to the ACOT(χ) prescription, the lowest order φ -independent cross section is

$$\sigma_2^{(LO)}(x, \lambda) = \int_{\chi}^1 dz g(z, \mu_F) \left[\hat{\sigma}_{2,g}^{(0)}(x/z, \lambda) - \frac{\alpha_s}{\pi} \ln \frac{\mu_F^2}{m^2} \hat{\sigma}_B(x/z) P_{g \rightarrow c}^{(0)}(\chi/z) \right] + \hat{\sigma}_B(x) c_+(\chi, \mu_F), \quad (54)$$

where $P_{g \rightarrow c}^{(0)}$ is the LO gluon-quark splitting function, $P_{g \rightarrow c}^{(0)}(\zeta) = [(1 - \zeta)^2 + \zeta^2]/2$, and the LO GF cross section $\hat{\sigma}_{2,g}^{(0)}$ is given by Eqs. (39). Remember also that $\chi = x(1 + 4\lambda)$ and $c_+(\zeta, \mu_F) = c(\zeta, \mu_F) + \bar{c}(\zeta, \mu_F)$.

The asymptotic behavior of the subtraction terms is fixed by the parton level factorization theorem. This theorem implies that the partonic cross sections $d\hat{\sigma}$ can be factorized into process-dependent infra-red safe hard scattering cross sections $d\tilde{\sigma}$, which are finite in the limit $m \rightarrow 0$, and universal (process-independent) partonic PDFs $f_{a \rightarrow i}$ and fragmentation functions $d_{n \rightarrow Q}$:

$$d\hat{\sigma}(\gamma^* + a \rightarrow Q + X) = \sum_{i,n} f_{a \rightarrow i}(\zeta) \otimes d\tilde{\sigma}(\gamma^* + i \rightarrow n + X) \otimes d_{n \rightarrow Q}(z). \quad (55)$$

In Eq. (55), the symbol \otimes denotes the usual convolution integral, the indices a, i, n and Q denote partons, $p_i = \zeta p_a$ and $p_Q = z p_n$. All the logarithms of the heavy-quark mass (i.e., the singularities in the limit $m \rightarrow 0$) are contained in the PDFs $f_{a \rightarrow i}$ and fragmentation functions $d_{n \rightarrow Q}$ while $d\tilde{\sigma}$ are IR-safe (i.e., are free of the $\ln m^2$ terms). The expansion of Eq. (55) can be used to determine order by order the subtraction terms. In particular, for the LO GF contribution to the charm leptoproduction one finds [6]

$$\hat{\sigma}_{k,SUB}^{(0)}(z, \ln(\mu_F^2/m^2)) = f_{g \rightarrow c}^{(1)}(\zeta, \ln(\mu_F^2/m^2)) \otimes \hat{\sigma}_{k,QS}^{(0)}(z/\zeta), \quad (k = 2, L, A, I), \quad (56)$$

where $f_{g \rightarrow c}^{(1)}(\zeta, \ln(\mu_F^2/m^2)) = (\alpha_s/2\pi) \ln(\mu_F^2/m^2) P_{g \rightarrow c}^{(0)}(\zeta)$ describes the charm distribution in the gluon within the $\overline{\text{MS}}$ factorization scheme.

One can see from Eq. (56) that the azimuth-dependent GF cross sections $\hat{\sigma}_{A,GF}$ and $\hat{\sigma}_{I,GF}$ don't have subtraction terms at LO because the lowest order QS contribution is φ -independent. For this reason, the $\cos 2\varphi$ -dependence within the VFNS has the same form as in the FFNS:

$$\sigma_A^{(LO)}(x, \lambda) = \int_{\chi}^1 dz g(z, \mu_F) \hat{\sigma}_{A,g}^{(0)}(x/z, \lambda). \quad (57)$$

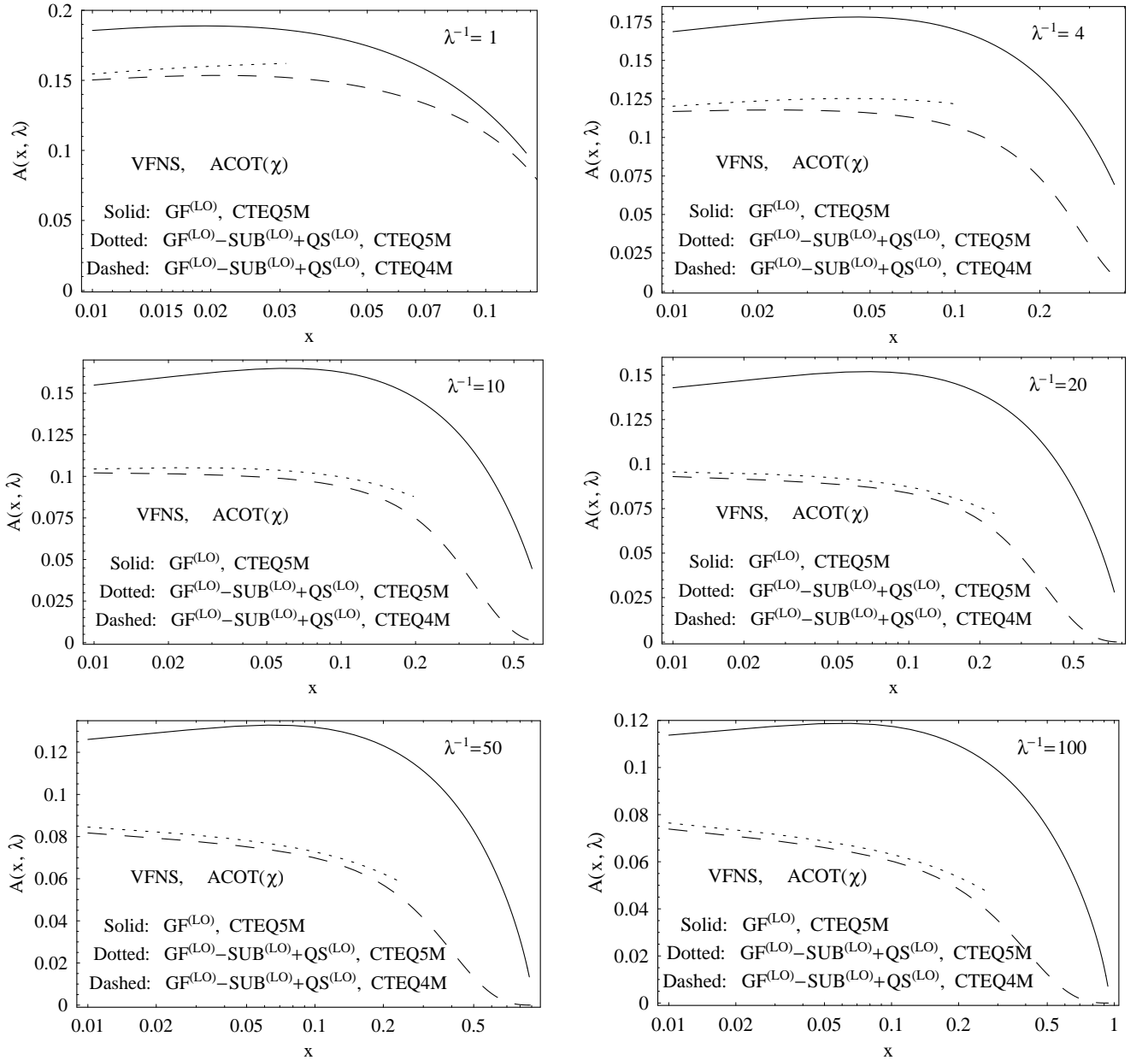


FIG. 8: Azimuthal asymmetry parameter $A(x, \lambda)$ in the VFNS at several values of λ . The following contributions are plotted: $GF^{(LO)}$ (solid curves), $GF^{(LO)} - SUB^{(LO)} + QS^{(LO)}$ with the CTEQ5M set of PDFs (dotted curves) and $GF^{(LO)} - SUB^{(LO)} + QS^{(LO)}$ with the CTEQ4M set of PDFs (dashed curves).

Fig. 8 shows the $ACOT(\chi)$ predictions for the asymmetry parameter $A(x, \lambda)$ at several values of variable λ : $\lambda^{-1} = 1, 4, 10, 20, 50$ and 100 . For comparison, we plot also the LO GF predictions (solid curves). In the $ACOT(\chi)$ case, we consider the CTEQ5M (dotted lines) and CTEQ4M (dashed curves) parametrizations of the gluon and charm densities in the proton. Corresponding values of the charm quark mass are $m_c = 1.3$ GeV [40] (for the CTEQ5M PDFs) and $m_c = 1.6$ GeV [44] (for the CTEQ4M PDFs). The default value of the factorization scale is $\mu_F = \sqrt{m^2 + Q^2}$.

One can see from Fig. 8 the following properties of the azimuthal asymmetry, $A(x, \lambda)$, within the VFNS. Contrary to the nonperturbative IC component, the perturbative one is significant practically at all values of Bjorken x and $Q^2 > m^2$. The perturbative charm contribution leads to a sizeable decreasing of the GF predictions for the $\cos 2\varphi$ -asymmetry. In the $ACOT(\chi)$ scheme, the IC contribution reduces the GF results for $A(x, \lambda)$ by about 30%. The origin of this reduction is straightforward: the QS component is practically $\cos 2\varphi$ -independent.

The ACOT(χ) predictions for the asymmetry depend weakly on the parton distribution functions we use. It is seen from Fig. 8 that the CTEQ5M and CTEQ4M sets of PDFs lead to very similar results for $A(x, \lambda)$. Note that we give the CTEQ5M predictions at low x only because of irregularities in the CTEQ5M charm density at large x .

We have also analyzed how the VFNS predictions depend on the choice of subtraction prescription. In particular, the schemes proposed in Refs. [26, 45] have been considered. We find that, sufficiently above the production threshold, these subtraction prescriptions reduce the GF results for the asymmetry by approximately 30 \div 50%.

One can conclude that impact of the perturbative IC on the $\cos 2\varphi$ asymmetry is essential in the whole region of Bjorken x and therefore can be tested experimentally.

IV. CONCLUSION

In the present paper, we consider the azimuthal dependence in charm leptoproduction as a probe of the IC content of the proton. Our analysis is based on the fact that the GF and QS components have strongly different $\cos 2\varphi$ -distributions. This fact follows from the NLO calculations of both parton level contributions. In the framework of the FFNS, we justify the most remarkable property of the hadron level azimuthal $\cos 2\varphi$ asymmetry: the combined GF+QS predictions for $A(x, Q^2)$ are perturbatively and parametrically stable. The nonperturbative IC contribution (resulting from the five-quark $|uudcc\bar{c}\rangle$ component of the proton wave function) is practically invisible at low x , but affects essentially the GF predictions for the asymmetry at large Bjorken x . We conclude that measurements of the $\cos 2\varphi$ asymmetry at large x could directly probe the nonperturbative intrinsic charm.

Within the VFNS, charm density originates perturbatively from the $g \rightarrow c\bar{c}$ process and obeys the DGLAP evolution equation. Presently, charm densities are included practically in all the global sets of PDFs like CTEQ and MRST. Our analysis shows that these charm distribution functions reduce dramatically (by about 1/3) the GF predictions for $A(x, Q^2)$ practically at all values of x . For this reason, the perturbative IC contribution can easily be measured using the azimuthal $\cos 2\varphi$ -distributions in charm leptoproduction.

The VFNS schemes have been proposed to resum the mass logarithms of the form $\alpha_s^n \ln^n(Q^2/m^2)$ which dominate the production cross sections at high energies. Evidently, were the calculation done to all orders of α_s , the VFNS and FFNS (without nonperturbative IC) would be exactly equivalent. There is a point of view advocated in Refs. [6, 7] that, at high energies, the perturbative series converge better within the VFNS than in the FFNS. There is also another opinion [46, 47] that the above logarithms do not vitiate the convergence of the perturbation expansion so that a resummation is, in principle, not necessary. Our analysis of the azimuthal dependence in leptoproduction indicates an experimental way to resolve this problem. First, contrary to the production cross sections, the azimuthal $\cos 2\varphi$ -asymmetry is well defined numerically in pQCD. Second, sufficiently above the production threshold (i.e., at small enough Bjorken x), the LO VFNS predictions for the $\cos 2\varphi$ -asymmetry differ by more than 30% from the corresponding FFNS ones. Third, nonperturbative contributions (like the intrinsic gluon motion in the target) can't compensate for this difference at non-small Q^2 where the VFNS is expected to be adequate. Therefore measurements of the azimuthal distributions in charm leptoproduction would make it possible to clarify the question whether the VFNS perturbative series for $A(x, Q^2)$ converges better than the FFNS one.

Acknowledgments

We thank S.J. Brodsky for stimulating discussions and useful suggestions. We also would like to acknowledge interesting correspondence with I. Schienbein. This work was supported in part by the ANSEF grant 04-PS-hepth-813-98 and NFSAT grant GRSP-16/06.

APPENDIX A: VIRTUAL AND SOFT CONTRIBUTIONS TO THE QUARK SCATTERING

In this Appendix we reproduce some results of Hoffmann and Moore for the φ -independent QS cross sections, and correct two misprints uncovered in Ref. [25]. We work in four dimensions, in the Feynman gauge and use the on-mass-shell renormalization scheme. We compute the absorptive part of the Feynman diagram (which is free of the UV divergences) and then restore the real part using the appropriate dispersion relations.

In the on-mass-shell scheme, the renormalized fermion self-energy vanishes like $(\hat{p}_Q - m)^2$ which means that the second and third diagrams in Fig. 2c do not contribute to the cross section when the external quark legs are on-shell,

$\hat{p}_Q \rightarrow m$. The first graph in Fig. 2c describes the NLO corrections to the quark-photon vertex function:

$$\Lambda_\mu(q) = f(Q^2) \gamma_\mu - \frac{g(Q^2)}{2m} \sigma_{\mu\nu} q^\nu, \quad (\text{A1})$$

where $\sigma_{\mu\nu} = \frac{1}{2} (\gamma_\mu \gamma_\nu - \gamma_\nu \gamma_\mu)$ while $f(Q^2)$ and $g(Q^2)$ are the quark electromagnetic formfactors. At the lowest order $\Lambda_\mu^{(0)} = \gamma_\mu$.

The virtual lepton-quark cross section, $\hat{\sigma}_{lQ}^V$, is obtained from the interference term between the virtual and the Born amplitude. The result can be written in terms of the electromagnetic formfactors as:

$$\frac{d^2 \hat{\sigma}_{lQ}^V}{dz dQ^2} = \frac{\alpha_{em}}{\pi} \frac{\hat{\sigma}_B(z)}{z Q^2} \delta(1-z) \{ [1 + (1-y)^2 - 2\lambda z^2 y^2] f(Q^2) + y^2 g(Q^2) \}. \quad (\text{A2})$$

Taking into account the definition of the HM cross sections, $\sigma^{(2)}$ and $\sigma^{(L)}$, given by Eqs. (33), (34) and (16), we find that corresponding virtual parts are:

$$\sigma_{1V}^{(2)}(z, Q^2) = 2\delta(1-z)f^{(1)}(Q^2), \quad \sigma_{1V}^{(L)}(z, Q^2) = -\delta(1-z)g^{(1)}(Q^2), \quad (\text{A3})$$

where $f^{(1)}(Q^2)$ and $g^{(1)}(Q^2)$ are the NLO corrections to the electromagnetic formfactors. For the NLO HM cross sections, $\sigma_{1V}^{(2)}$ and $\sigma_{1V}^{(L)}$, we use exactly the same notations as in Ref. [25].

In the on-mass-shell renormalization scheme, the renormalized vertex correction vanishes as the photon virtuality goes to zero, $f^{(1)}(0) = 0$. This is a consequence of the Ward identity and the fact that the real photon field (like the massive fermion one) is unrenormalized in first order QCD. To satisfy the condition $f^{(1)}(0) = 0$ automatically, we should use for $f^{(1)}(q^2)$ the dispersion relation with one subtraction. The second formfactor, $g^{(1)}(q^2)$, has no singularities. For this reason, we use for $g^{(1)}(q^2)$ the dispersion relation without subtractions:

$$f^{(1)}(q^2) = \frac{q^2}{\pi} \int_{4m^2}^{\infty} \frac{dt \operatorname{Im} f^{(1)}(t)}{t(t - q^2 - i0)}, \quad g^{(1)}(q^2) = \frac{1}{\pi} \int_{4m^2}^{\infty} \frac{dt \operatorname{Im} g^{(1)}(t)}{t - q^2 - i0}. \quad (\text{A4})$$

Calculating the imaginary parts of the formfactors and restoring their real parts with the help of Eqs. (A4) yields

$$f^{(1)}(Q^2) = \frac{\alpha_s}{\pi} C_F \left\{ \left[1 + \frac{1+2\lambda}{\sqrt{1+4\lambda}} \ln r \right] \left(\ln \frac{m}{m_g} - 1 \right) + \frac{1+2\lambda}{\sqrt{1+4\lambda}} \left[\operatorname{Li}_2(-r) + \frac{\pi^2}{12} + \frac{1}{4} \ln^2 r + \frac{1}{2} \ln r \ln \frac{1+4\lambda}{\lambda} \right] + \frac{1}{4} \frac{\ln r}{\sqrt{1+4\lambda}} \right\}, \quad (\text{A5})$$

$$g^{(1)}(Q^2) = -\frac{\alpha_s}{\pi} C_F \frac{\lambda \ln r}{\sqrt{1+4\lambda}}. \quad (\text{A6})$$

In Eqs. (A5) and (A6), $C_F = (N_c^2 - 1)/(2N_c)$, where N_c is number of colors, and r is defined by Eq. (27). Taking into account that $\Lambda^{(1)\mu} = (\alpha_s/\alpha_{em}) C_F \Lambda_{QED}^{(1)\mu}$, we see that Eqs. (A5, A6) reproduce the textbook QED results.

It is now straightforward to obtain the virtual contribution to the longitudinal cross section. Combining Eqs. (A3) and (A6) yields:

$$\sigma_{1V}^{(L)}(z, Q^2) = \frac{\alpha_s}{\pi} C_F \delta(1-z) \frac{\lambda \ln r}{\sqrt{1+4\lambda}}. \quad (\text{A7})$$

Comparing the above result with the corresponding one given by Eq. (39) in Ref. [25], we see that the HM expression for $\sigma_{1V}^{(L)}$ has opposite sign. Note also that this typo propagates into the final result for $\sigma_1^{(L)}$ given by Eq. (52) [25].

Calculation of the bremsstrahlung contribution to the longitudinal cross section, $\sigma_{1B}^{(L)}(z, Q^2)$, is also straightforward. We coincide with the HM result for $\sigma_{1B}^{(L)}(z, Q^2)$ given by Eq. (49) in Ref. [25]. However there is one more misprint in the HM expression for $\sigma_1^{(L)}$: the r.h.s of Eq. (52) [25] should be multiplied by z .

In the case of $\sigma_1^{(2)}(z, Q^2)$, the situation is slightly more complicated due to the need to take into account the IR singularities. One can see from Eq. (A5) that $f^{(1)}(Q^2)$ has an IR divergence which is regularized with the help of an infinitesimal gluon mass m_g . This singularity is cancelled when one adds the so-called soft contribution originating

from the real gluon emission. For this purpose we introduce another infinitesimal parameter δz , $(m_g/m) \ll \delta z \ll 1$. The full bremsstrahlung contribution, $\sigma_{1B}^{(2)}$, can then be splitted into the soft and hard pieces as follows:

$$\sigma_{1soft}^{(2)}(z, Q^2) = \theta(z + \delta z - 1)\sigma_{1B}^{(2)}(z, Q^2), \quad \sigma_{1hard}^{(2)}(z, Q^2) = \theta(1 - z - \delta z)\sigma_{1B}^{(2)}(z, Q^2), \quad (A8)$$

where $\theta(1 - z - \delta z)$ is the Heaviside step function. The soft cross section should be calculated in the eikonal approximation, $\vec{p}_g \rightarrow 0$, taking into account the infinitesimal gluon mass m_g . As a result, the sum of the virtual and soft contributions is IR finite:

$$\begin{aligned} \sigma_{1V}^{(2)} + \sigma_{1soft}^{(2)} &= \frac{\alpha_s}{\pi} C_F \delta(1 - z) \left\{ -2 \ln(\delta z) \left[1 + \frac{1 + 2\lambda}{\sqrt{1 + 4\lambda}} \ln r \right] + 2 \ln \lambda - 1 - \frac{\sqrt{1 + 4\lambda}}{2} \ln r \right. \\ &\quad \left. + \frac{1 + 2\lambda}{\sqrt{1 + 4\lambda}} \left[\text{Li}_2(r^2) + 2\text{Li}_2(-r) + \frac{3}{2} \ln^2 r - 2 \ln r - \ln r \ln \lambda + 2 \ln r \ln(1 + 4\lambda) \right] \right\}. \end{aligned} \quad (A9)$$

Adding to the above expression the hard cross section $\sigma_{1hard}^{(2)}$ defined by Eq. (A8), we reproduce in the limit $\delta z \rightarrow 0$ the full result for $\sigma_1^{(2)}$ given by Eq. (51) in Ref. [25].

APPENDIX B: NLO SOFT-GLUON CORRECTIONS TO THE PHOTON-GLUON FUSION

This Appendix provides an overview of the NLO soft-gluon approximation for the photon-gluon fusion mechanism. We present the final results for the parton level cross sections to the next-to-leading logarithmic (NLL) accuracy. More details can be found in Refs. [20, 21, 39].

To take into account the NLO contributions to the GF mechanism, one needs to calculate the virtual $\mathcal{O}(\alpha_{em}\alpha_s^2)$ corrections to the Born process (38) and the real gluon emission:

$$\gamma^*(q) + g(k_g) \rightarrow Q(p_Q) + \bar{Q}(p_{\bar{Q}}) + g(p_g). \quad (B1)$$

The partonic invariants describing the single-particle inclusive (1PI) kinematics are

$$\begin{aligned} s' &= 2q \cdot k_g = s + Q^2 = \zeta S', & t_1 &= (k_g - p_Q)^2 - m^2 = \zeta T_1, \\ s_4 &= s' + t_1 + u_1, & u_1 &= (q - p_Q)^2 - m^2 = U_1, \end{aligned} \quad (B2)$$

where ζ is defined by $\vec{k}_g = \zeta \vec{p}$ and s_4 measures the inelasticity of the reaction (B1). The corresponding 1PI hadron level variables describing the reaction (1) are

$$\begin{aligned} S' &= 2q \cdot p = S + Q^2, & T_1 &= (p - p_Q)^2 - m^2, \\ S_4 &= S' + T_1 + U_1, & U_1 &= (q - p_Q)^2 - m^2. \end{aligned} \quad (B3)$$

The exact NLO calculations of the unpolarized heavy quark production in γg [48, 49], $\gamma^* g$ [38], and gg [50, 51, 52, 53] collisions show that, near the partonic threshold, a strong logarithmic enhancement of the cross sections takes place in the collinear, $\vec{p}_{g,T} \rightarrow 0$, and soft, $\vec{p}_g \rightarrow 0$, limits. This threshold (or soft-gluon) enhancement has universal nature in the perturbation theory and originates from incomplete cancellation of the soft and collinear singularities between the loop and the bremsstrahlung contributions. Large leading and next-to-leading threshold logarithms can be resummed to all orders of perturbative expansion using the appropriate evolution equations [54, 55, 56]. The analytic results for the resummed cross sections are ill-defined due to the Landau pole in the coupling strength α_s . However, if one considers the obtained expressions as generating functionals of the perturbative theory and re-expands them at fixed order in α_s , no divergences associated with the Landau pole are encountered.

Soft-gluon resummation for the photon-gluon fusion has been performed in Ref. [39] and checked in Refs. [20, 21]. To NLL accuracy, the perturbative expansion for the partonic cross sections, $d^2\hat{\sigma}_{k,g}/dt_1 du_1$ ($k = T, L, A, I$), can be written in a factorized form as

$$s'^2 \frac{d^2\hat{\sigma}_{k,g}}{dt_1 du_1}(s', t_1, u_1) = B_{k,g}^{\text{Born}}(s', t_1, u_1) \left\{ \delta(s' + t_1 + u_1) + \sum_{n=1}^{\infty} \left(\frac{\alpha_s C_A}{\pi} \right)^n K^{(n)}(s', t_1, u_1) \right\}, \quad (B4)$$

with the Born level distributions $B_{k,g}^{\text{Born}}$ given by

$$\begin{aligned}
B_{T,g}^{\text{Born}}(s', t_1, u_1) &= \pi e_Q^2 \alpha_{em} \alpha_s \left[\frac{t_1}{u_1} + \frac{u_1}{t_1} + 4 \left(\frac{s}{s'} - \frac{m^2 s'}{t_1 u_1} \right) \left(\frac{s'(m^2 - Q^2/2)}{t_1 u_1} + \frac{Q^2}{s'} \right) \right], \\
B_{L,g}^{\text{Born}}(s', t_1, u_1) &= \pi e_Q^2 \alpha_{em} \alpha_s \left[\frac{8Q^2}{s'} \left(\frac{s}{s'} - \frac{m^2 s'}{t_1 u_1} \right) \right], \\
B_{A,g}^{\text{Born}}(s', t_1, u_1) &= \pi e_Q^2 \alpha_{em} \alpha_s \left[4 \left(\frac{s}{s'} - \frac{m^2 s'}{t_1 u_1} \right) \left(\frac{m^2 s'}{t_1 u_1} + \frac{Q^2}{s'} \right) \right], \\
B_{I,g}^{\text{Born}}(s', t_1, u_1) &= \pi e_Q^2 \alpha_{em} \alpha_s \left[4 \sqrt{Q^2} \left(\frac{t_1 u_1 s}{s'^2} - m^2 \right)^{1/2} \frac{t_1 - u_1}{t_1 u_1} \left(1 - \frac{2Q^2}{s'} - \frac{2m^2 s'}{t_1 u_1} \right) \right].
\end{aligned} \tag{B5}$$

Note that the functions $K^{(n)}(s', t_1, u_1)$ in Eq. (B4) originate from the collinear and soft limits. Radiation of soft and collinear gluons does not affect the transverse momentum of detected particles and therefore the azimuthal angle φ . For this reason, the functions $K^{(n)}(s', t_1, u_1)$ are the same for all helicity cross sections $\hat{\sigma}_{k,g}$ ($k = T, L, A, I$). At NLO, the soft-gluon corrections to NLL accuracy in the $\overline{\text{MS}}$ scheme are

$$\begin{aligned}
K^{(1)}(s', t_1, u_1) &= 2 \left[\frac{\ln(s_4/m^2)}{s_4} \right]_+ - \left[\frac{1}{s_4} \right]_+ \left\{ 1 + \ln \left(\frac{u_1}{t_1} \right) - \left(1 - \frac{2C_F}{C_A} \right) (1 + \text{Re}L_\beta) + \ln \left(\frac{\mu^2}{m^2} \right) \right\} \\
&\quad + \delta(s_4) \ln \left(\frac{-u_1}{m^2} \right) \ln \left(\frac{\mu^2}{m^2} \right),
\end{aligned} \tag{B6}$$

where we use $\mu = \mu_F = \mu_R$. In Eq. (B6), $C_A = N_c$ and $C_F = (N_c^2 - 1)/(2N_c)$, where N_c is number of colors, while $L_\beta = (1 - 2m^2/s)\{\ln[(1 - \beta)/(1 + \beta)] + i\pi\}$ with $\beta = \sqrt{1 - 4m^2/s}$. The single-particle inclusive "plus" distributions are defined by

$$\left[\frac{\ln^l(s_4/m^2)}{s_4} \right]_+ = \lim_{\epsilon \rightarrow 0} \left\{ \frac{\ln^l(s_4/m^2)}{s_4} \theta(s_4 - \epsilon) + \frac{1}{l+1} \ln^{l+1} \left(\frac{\epsilon}{m^2} \right) \delta(s_4) \right\}. \tag{B7}$$

For any sufficiently regular test function $h(s_4)$, Eq. (B7) gives

$$\int_0^{s_4^{\text{max}}} ds_4 h(s_4) \left[\frac{\ln^l(s_4/m^2)}{s_4} \right]_+ = \int_0^{s_4^{\text{max}}} ds_4 [h(s_4) - h(0)] \frac{\ln^l(s_4/m^2)}{s_4} + \frac{1}{l+1} h(0) \ln^{l+1} (s_4^{\text{max}}/m^2). \tag{B8}$$

In Eq. (B6), we have preserved the NLL terms for the scale-dependent logarithms too. Note also that the results (B5) and (B6) agree to NLL accuracy with the exact $\mathcal{O}(\alpha_{em} \alpha_s^2)$ calculations of the photon-gluon cross sections $\hat{\sigma}_{T,g}$ and $\hat{\sigma}_{L,g}$ given in Ref. [38].

To investigate the scale dependence of the results (B4–B6), it is convenient to introduce for the fully inclusive (integrated over t_1 and u_1) cross sections, $\hat{\sigma}_{k,g}$ ($k = T, L, A, I$), the dimensionless coefficient functions $c_{k,g}^{(n,l)}$ defined by Eq. (30). Concerning the NLO scale-independent coefficient functions, only $c_{T,g}^{(1,0)}$ and $c_{L,g}^{(1,0)}$ are known exactly [38, 57]. As to the μ -dependent coefficients, they can be calculated explicitly using the evolution equation:

$$\frac{d\hat{\sigma}_{k,g}(z, Q^2, \mu^2)}{d \ln \mu^2} = - \int_{\zeta_{\text{min}}}^1 d\zeta \hat{\sigma}_{k,g}(z/\zeta, Q^2, \mu^2) P_{gg}(\zeta), \tag{B9}$$

where $z = Q^2/s'$, $\zeta_{\text{min}} = z(1 + 4\lambda)$, $\hat{\sigma}_{k,g}(z, Q^2, \mu)$ are the cross sections resummed to all orders in α_s and $P_{gg}(\zeta)$ is the corresponding (resummed) Altarelli-Parisi gluon-gluon splitting function. Expanding Eq. (B9) in α_s , one can find [20, 39]

$$c_{k,g}^{(1,1)}(z, \lambda) = \frac{1}{4\pi^2} \int_{\zeta_{\text{min}}}^1 d\zeta \left[b_2 \delta(1 - \zeta) - P_{gg}^{(0)}(\zeta) \right] c_{k,g}^{(0,0)}(z/\zeta, \lambda), \tag{B10}$$

where $b_2 = (11C_A - 2n_f)/12$ is the first coefficient of the $\beta(\alpha_s)$ -function expansion and n_f is the number of active quark flavors. The one-loop gluon splitting function is:

$$P_{gg}^{(0)}(\zeta) = \lim_{\epsilon \rightarrow 0} \left\{ \left(\frac{\zeta}{1-\zeta} + \frac{1-\zeta}{\zeta} + \zeta(1-\zeta) \right) \theta(1-\zeta-\epsilon) + \delta(1-\zeta) \ln \epsilon \right\} C_A + b_2 \delta(1-\zeta). \quad (\text{B11})$$

With Eq. (B10) in hand, it is possible to check the quality of the NLL approximation against exact answers. As shown in Ref. [21], the soft-gluon corrections reproduce satisfactorily the threshold behavior of the available exact results for $\lambda \sim 1$. Since the gluon distribution function supports just the threshold region, the soft-gluon contribution dominates the photon-hadron cross sections $\sigma_{k,GF}$ ($k = T, L, A, I$) at energies not so far from the production threshold and at relatively low virtuality $Q^2 \lesssim m^2$.

APPENDIX C: NONPERTURBATIVE IC AND RELEVANT EXPERIMENTAL FACTS

The most clean probe of the charm quark distribution function (both perturbative and nonperturbative) is the semi-inclusive deep inelastic lepton-proton scattering, $l p \rightarrow l' c X$. To measure the nonperturbative IC contribution, one needs data on the charm production at sufficiently large Bjorken x . The only experiment which has investigated the large x domain is the European Muon Collaboration (EMC) [58] where the decay lepton spectra have been used to detect the produced charmed particles. In Ref. [59], a re-analysis of the EMC data on $F_2^c(x, Q^2)$ have been performed using the NLO results for both GF and QS components. The analysis [59] shows that a nonperturbative intrinsic charm contribution to the proton wave function of the order of 1% is needed to fit the EMC data in the large x region. This value of the nonperturbative IC is consistent with the estimates based on the operator product expansion [5]. Note however that the EMC data are of limited statistics and, for this reason, more accurate measurements of charm leptoproduction at large x are necessary.

It is also possible to extract useful information on the IC from diffractive dissociation processes such as $p \rightarrow p J/\psi$ on a nuclear target. Comprehensive measurements of the $pA \rightarrow J/\psi X$ and $\pi A \rightarrow J/\psi X$ cross sections have been performed in the fixed target experiments NA3 at CERN [60] and E886 at FNAL [61]. According to the arguments presented in Refs. [62, 63, 64], the IC contribution is predicted to be strongly shadowed in the above reactions that is in a complete agreement with the observed nuclear dependence of the high Feynman x_F component of the J/ψ hadroproduction.

A non-vanishing five-quark Fock component $|uudc\bar{c}\rangle$ leads to the production of open charm states such as $\Lambda_c(cud)$ and $D^-(\bar{c}d)$ with large Feynman x_F . This may occur either through a coalescence of the valence and charm quarks which are moving with the same rapidity or via hadronization of the produced c and \bar{c} . As shown in Refs. [65, 66], a model based on the nonperturbative intrinsic charm naturally explains the leading particle effect in the $pp \rightarrow DX$ and $pp \rightarrow \Lambda_c X$ processes that has been observed at the ISR [67] and Fermilab [68, 69].

As to the high- x_F hadroproduction of open bottom states like $\Lambda_b(bud)$, corresponding cross sections are predicted to be suppressed as $m_c^2/m_b^2 \sim 1/10$ in comparison with the case of charm production. Evidence for the forward Λ_b production in the pp collisions at the ISR energy was reported in Refs. [70, 71].

Rare seven-quark fluctuations of the type $|uudc\bar{c}c\bar{c}\rangle$ in the proton wave function can lead to the production of two J/ψ [72] or a double-charm baryon state at large x_F and low p_T . Double J/ψ events with a high combined $x_F \geq 0.5$ have been detected in the NA3 experiment [73]. An observation of the double-charmed baryon $\Xi_{cc}^+(3520)$ with mean $\langle x_F \rangle \simeq 0.33$ has been reported by the SELEX collaboration at FNAL [74].

[1] S. J. Brodsky, P. Hoyer, C. Peterson, and N. Sakai, Phys. Lett. B **93**, 451 (1980).
[2] S. J. Brodsky, C. Peterson, and N. Sakai, Phys. Rev. D **23**, 2745 (1981).
[3] S. J. Brodsky, "Light-front QCD", hep-ph/0412101.
[4] S. J. Brodsky, Few Body Syst. **36**, 35 (2005).
[5] M. Franz, V. Polyakov, and K. Goeke, Phys. Rev. D **62**, 074024 (2000).
[6] M. A. G. Aivazis, J. C. Collins, F. I. Olness, and W. -K. Tung, Phys. Rev. D **50**, 3102 (1994).
[7] J. C. Collins, Phys. Rev. D **58**, 094002 (1998).
[8] V. N. Gribov and L. N. Lipatov, Sov. J. Nucl. Phys. **15**, 438 (1972).
[9] Y. L. Dokshitzer, Sov. Phys. JETP **46**, 641 (1977).
[10] G. Altarelli and G. Parisi, Nucl. Phys. B **126**, 298 (1977).
[11] J. Pumplin, Phys. Rev. D **73**, 114015 (2006).
[12] S. J. Brodsky, B. Kopeliovich, I. Schmidt, and J. Soffer, Phys. Rev. D **73**, 113005 (2006).
[13] J. Pumplin, D. R. Stump, J. Huston, H. L. Lai, P. Nadolsky, and W. K. Tung, JHEP **0207**, 012 (2002).

[14] A. D. Martin, R. G. Roberts, W. J. Stirling, and R. S. Thorne, *Phys. Lett. B* **604**, 61 (2004).

[15] N. Kidonakis, *Phys. Rev. D* **73**, 034001 (2006).

[16] N. Kidonakis, *Phys. Rev. D* **64**, 014009 (2001).

[17] M. L. Mangano, P. Nason, and G. Ridolfi, *Nucl. Phys. B* **373**, 295 (1992).

[18] S. Frixione, M. L. Mangano, P. Nason, and G. Ridolfi, *Nucl. Phys. B* **412**, 225 (1994).

[19] N. Ya. Ivanov, A. Capella, and A. B. Kaidalov, *Nucl. Phys. B* **586**, 382 (2000).

[20] N. Ya. Ivanov, *Nucl. Phys. B* **615**, 266 (2001).

[21] N. Ya. Ivanov, *Nucl. Phys. B* **666**, 88 (2003).

[22] N. Ya. Ivanov, P. E. Bosted, K. Griffioen, and S. E. Rock, *Nucl. Phys. B* **650**, 271 (2003).

[23] SLAC E161 (2000), <http://www.slac.stanford.edu/exp/e160>.

[24] N. Dombey, *Rev. Mod. Phys.* **41**, 236 (1969).

[25] E. Hoffman and R. Moore, *Z. Phys. C* **20**, 71 (1983).

[26] S. Kretzer and I. Schienbein, *Phys. Rev. D* **58**, 094035 (1998).

[27] A. Deshpande, R. Milner, R. Venugopalan, and W. Vogelsang, *Ann. Rev. Nucl. Part. Sci.* **55**, 165 (2005).

[28] See also <http://www.bnl.gov/eic> for information concerning the eRHIC/EIC project.

[29] J. B. Dainton, M. Klein, P. Newman, E. Perez, and F. Willeke, [hep-ex/0603016](https://arxiv.org/abs/hep-ex/0603016).

[30] L. N. Ananikyan and N. Ya. Ivanov, [hep-ph/0609074](https://arxiv.org/abs/hep-ph/0609074).

[31] I. Schienbein, [hep-ph/0110292](https://arxiv.org/abs/hep-ph/0110292).

[32] H. Georgi and H. D. Politzer, *Phys. Rev. Lett.* **40**, 3 (1978).

[33] A. Méndez, *Nucl. Phys. B* **145**, 199 (1978).

[34] U. Fano, *Phys. Rev.* **93**, 121 (1954).

[35] J. P. Leveille and T. Weiler, *Phys. Rev. D* **24**, 1789 (1981).

[36] A. D. Watson, *Z. Phys. C* **12**, 123 (1982).

[37] J. P. Leveille and T. Weiler, *Nucl. Phys. B* **147**, 147 (1979).

[38] E. Laenen, S. Riemersma, J. Smith, and W. L. van Neerven, *Nucl. Phys. B* **392**, 162 (1993).

[39] E. Laenen and S. -O. Moch, *Phys. Rev. D* **59**, 034027 (1999).

[40] H. L. Lai et al., *Eur. Phys. J. C* **12**, 375 (2000).

[41] L. Apanasevich et al., *Phys. Rev. D* **59**, 074007 (1999).

[42] M. A. G. Aivazis, F. I. Olness, and W. -K. Tung, *Phys. Rev. D* **50**, 3085 (1994).

[43] W. -K. Tung, S. Kretzer, and C. Schmidt, *J. Phys. G* **28**, 983 (2002).

[44] H. L. Lai et al., *Phys. Rev. D* **55**, 1280 (1997).

[45] M. Kramer, F. I. Olness, and D. E. Soper, *Phys. Rev. D* **62**, 096007 (2000).

[46] W. L. van Neerven, [hep-ph/0107193](https://arxiv.org/abs/hep-ph/0107193).

[47] M. Buza, Y. Matiounine, J. Smith, and W. L. van Neerven, *Eur. Phys. J. C* **1**, 301 (1998).

[48] R. K. Ellis and P. Nason, *Nucl. Phys. B* **312**, 551 (1989).

[49] J. Smith and W. L. van Neerven, *Nucl. Phys. B* **374**, 36 (1992).

[50] W. Beenakker, H. Kuijf, W. L. van Neerven, and J. Smith, *Phys. Rev. D* **40**, 54 (1989).

[51] P. Nason, S. Dawson, and R. K. Ellis, *Nucl. Phys. B* **303**, 607 (1988).

[52] P. Nason, S. Dawson, and R. K. Ellis, *Nucl. Phys. B* **327**, 49 (1989).

[53] P. Nason, S. Dawson, and R. K. Ellis, *Nucl. Phys. B* **335**, 260 (1990).

[54] H. Contopanagos, E. Laenen, and G. Sterman, *Nucl. Phys. B* **484**, 303 (1997).

[55] E. Laenen, G. Oderda, and G. Sterman, *Phys. Lett. B* **438**, 173 (1998).

[56] N. Kidonakis, G. Oderda, and G. Sterman, *Nucl. Phys. B* **531**, 365 (1998).

[57] B. W. Harris and J. Smith, *Nucl. Phys. B* **452**, 109 (1995).

[58] J. J. Aubert et al., *Nucl. Phys. B* **213**, 31 (1983).

[59] B. W. Harris, J. Smith, and R. Vogt, *Nucl. Phys. B* **461**, 181 (1996).

[60] J. Badier et al., *Z. Phys. C* **20**, 101 (1983).

[61] M. J. Leitch et al., *Phys. Rev. Lett.* **84**, 3256 (2000).

[62] S. J. Brodsky and P. Hoyer, *Phys. Rev. Lett.* **63**, 1566 (1989).

[63] P. Hoyer, M. Vanttilen, and U. Sukhatme, *Phys. Lett. B* **246**, 217 (1990).

[64] S. J. Brodsky, P. Hoyer, A. H. Mueller, and W. K. Tang, *Nucl. Phys. B* **369**, 519 (1992).

[65] V. D. Barger, F. Halzen, and W. Y. Keung, *Phys. Rev. D* **25**, 112 (1982).

[66] R. Vogt and S. J. Brodsky, *Nucl. Phys. B* **478**, 311 (1996).

[67] P. Chauvat et al., *Phys. Lett. B* **199**, 304 (1987).

[68] E. M. Aitala et al., *Phys. Lett. B* **495**, 42 (2000).

[69] E. M. Aitala et al., *Phys. Lett. B* **539**, 218 (2002).

[70] M. Basile et al., *Nuovo Cim. A* **65**, 408 (1981).

[71] G. Bari et al., *Nuovo Cim. A* **104**, 1787 (1991).

[72] R. Vogt and S. J. Brodsky, *Phys. Lett. B* **349**, 569 (1995).

[73] J. Badier et al., *Phys. Lett. B* **114**, 457 (1982).

[74] A. Ocherashvili et al., *Phys. Lett. B* **628**, 18 (2005).